Orbital current patterns in doped two-leg Cu-O Hubbard ladders

P. Chudzinski,[1] M. Gabay,[1] and T. Giamarchi[2]
[1]*Laboratoire de Physique des Solides, Bâtiment 510, Université Paris-Sud 11, Centre d'Orsay, 91405 Orsay Cedex, France*
[2]*DPMC-MaNEP, University of Geneva, 24 Quai Ernest-Ansermet, CH-1211 Geneva, Switzerland*
(Received 15 April 2008; published 28 August 2008)

In the weak-coupling limit, we investigate two-leg ladders with a unit cell containing both Cu and O atoms as a function of doping. For purely repulsive interactions, using bosonization, we find significant differences with the single-orbital case: a completely massless quantum critical regime is obtained for a finite range of carrier concentration. In a broad region of the phase diagram, the ground state consists of a pattern of orbital currents plus a density wave. NMR properties of the Cu and O nuclei are presented for the various phases.

DOI: 10.1103/PhysRevB.78.075124 PACS number(s): 71.27.+a, 71.10.Hf, 74.20.Mn

I. INTRODUCTION

Over the past two decades, the description of strongly correlated electron materials has been one of the most actively pursued problems in condensed-matter physics. When the strength of Coulomb interactions between carriers is on the order of (or larger than) their kinetic energy, many new remarkable phenomena may occur. Their fingerprints are seen in experiments done on systems such as cuprate compounds with high-temperature superconductivity,[1] cobaltites with large thermopower,[2] manganites with colossal magnetoresistance,[3] and heavy fermions.[4] Among these materials, cuprates play a special role. At half filling they are insulators with antiferromagnetic (AF) order, but with doping, a sequence of phases is observed including spin glass, pseudogap, *d*-type superconductivity (SCd), and eventually Fermi-type behavior for very large carrier concentrations.

Unfortunately there is, to date, no consensus on a theoretical model that would allow one to describe the physics of the Cu-O planes. In order to get insights into this strong correlation problem, the study of ladder structures[5,6] has proven quite useful. Ladders are the simplest systems that interpolate between one and two dimensions.[7] They constitute the quasi-one-dimensional analog of the Cu-O sheets and, because of the reduced dimensionality, even weak interactions lead to dramatic effects. In the one-dimensional (1D) case, the weak- and strong-interaction limits are usually smoothly connected.[8] Controlled nonperturbative methods—such as bosonization or conformal field theory—and numerical techniques can be used to analyze these systems.

Compounds characterized by a ladder structure,[5,6] such as SrCuO, have been synthesized. They show a variety of unusual properties, such as, for example, large magnetic fluctuations, SCd with purely repulsive interactions, and metal-insulator transitions under high pressure.[9–13] For these materials, increasing the pressure amounts to changing the bandwidth and hence the ratio of Coulomb to kinetic energies in the ladder structure.

These experimental developments provided a strong incentive for theorists to study two-leg ladders with Hubbard interactions between electrons. In the weakly interacting limit, renormalization-group (RG) analysis was used to explore their phase diagram.[14–22] Tsuchiizu and co-workers[23,24] performed an RG analysis in bosonization language in order to explore the regime of dopings close to half filling. Using current algebra, where spin-rotational symmetry was introduced *a priori* in order to derive RG equations, Balents and Fisher[20] and Lin *et al.*[21] established the phase diagram of two-leg ladder versus doping, showing that there is interesting physics at finite dopings. They identified a sequence of phases, labeled *CnSm* with n (m) gapless charge (spin) modes. Numerical density-matrix renormalization-group (DMRG) calculations focused on the large U limit,[25–27] the so-called t-J approximation at half filling.[28–30] The relevance of interchain hoppings on the low-energy physics was also addressed.[31–34]

The above-mentioned papers all assume that in the low-energy limit, the Cu-O system can be reduced to an effective single-orbital model. In the context of two-dimensional (2D) cuprate materials, such reduction to a single-orbital model was proposed by Zhang and Rice.[35] It allowed one to derive phase diagrams for these systems.[1,36] However this simplification was called into question, and it was pointed out that it is necessary to retain the full three-band nature of the model in order to capture the important physics.[37,38] This issue becomes particularly relevant when one examines the possible existence of orbital current phases. Such phases were initially proposed for the Hubbard model.[39] They were subsequently analyzed by various authors,[1,40–42] but in slave boson and in numerical calculations one finds that they are unstable. For single-band ladder models, controlled calculations appropriate to one dimension reveal that for special choices of interactions—which must include nonlocal terms—staggered flux patterns are stable. This phase breaks the translational symmetry of the lattice.[43–45] According to some authors,[1,46] the 2D version of this state [the *d*-density-wave (DDW) phase] describes the pseudogap phase of the cuprates. An alternative type of orbital current pattern, which preserves the lattice translational symmetry, was advocated to describe the pseudogap phase.[37,38] It then requires using a three-band model. Recent experimental data taken from neutron measurements[47] and polar Kerr effect[48] would be consistent with the latter proposal, but more studies are clearly needed to fully corroborate this scenario.

Motivated by these considerations, Lee *et al.*[49] (see also Ref. 50) generalized the system of RG equations written in current algebra language by Balents and Fisher[20] to study the Cu-O Hubbard ladder. Their work was, however, limited to the half-filled case, where umklapp terms dominate the phys-

ics, giving rise to Mott transitions. In a recent Rapid Communication,[51] we outlined the method which allowed us to map out the full diagram of the Cu-O ladder as a function of doping.

The aim of the present paper is to provide details of our derivation and to present additional results which are experimentally testable. In our work, oxygen atoms are taken into account at each calculation step, which allows us to probe their influence. First, they lead to additional types of phases compared with the single-orbital case: A Luttinger liquid (LL) regime is found for a finite range of dopings, and in a broad region of the phase diagram, the ground state displays an orbital current pattern plus density-wave quasi-long-range order. Our study thus underscores the importance of including these additional degrees of freedom in the structure, in particular with regards to the existence and to the stability of current patterns. Although our results have been derived for the specific case of ladders, they have potential relevance to the physics of 2D cuprate materials as well. Second, spectroscopic tools measuring local properties, such as NMR, are predicted to give different signatures depending on whether they probe Cu or O sites. In the large U limit, for 2D cuprates it is believed that spin fluctuations on oxygen sites merely track those on the copper sites.[36] The advantage of revisiting the issue in a quasi-1D context is that one can monitor spin excitations on oxygen atoms both in the small and the large U limits using bosonization techniques. This is done in the present paper for various dopings in the small U limit. We do find differences between the NMR signal on the copper and oxygen atoms at low temperature, when gaps set in, but not at higher temperature in the LL regime.

The paper is organized as follows: In Sec. II we define the model including the interactions relevant to the low-energy physics. In the continuum limit the quadratic part of the Hamiltonian is diagonal in a particular basis, B_o. We give the relations between this basis, the bonding/antibonding basis $B_{o\pi}$ (relevant in the noninteracting case), and the total/transverse density basis B_{+-} (the most appropriate for writing "backward" interactions).

In Sec. III we present an alternative method which allows one to set up the RG equations in the case of generic doping.[51] One of its salient features is that it treats the rotation of B_0 with respect to B_{+-} during the flow. This procedure allows us to perform calculations properly for *all dopings*. Indeed, symmetry requirements are fulfilled during the RG flows and our perturbative expansions remain controlled for a wide range of length scales. We list the resulting set of equations; their derivation is presented in Appendix B.

The various flows and the resulting phase diagram are given in Sec. IV. First we assess the impact of the additional degrees of freedom. Hence we set all Coulomb interactions pertaining to the O atoms and direct interoxygen hoppings to zero. Some of the results obtained in previous work[20] can now be checked using our improved RG method. In contrast with the single-orbital case, we find an intermediate doping range where all spin and gap modes are massless (i.e., a quantum critical line). Next, interactions involving oxygen atoms and hoppings between these atoms are introduced. We find that interoxygen hoppings promote a phase of orbital currents and we analyze its structure. Spin-rotational symmetry was not imposed *a priori*, but we checked that the required property was preserved during the flow. This provides a check on the consistency of our calculations. In the case of massive regimes, the evolution of the gaps with doping is shown. We briefly examine the impact of umklapp terms which are present at half filling.

Differences between the single- and multiorbital cases are discussed in detail in Sec. V A. The main point is that the presence of oxygen atoms changes initial parameters in such a way that certain symmetries [such as *particle-hole* symmetry at half filling or SU(2) pseudospin] are broken. This implies that rotations of the bases in the spin and in the charge sectors are independent in contradistinction with the case of the single-band two-leg ladder. Symmetry breaking has a direct influence on interaction terms and basis rotations on the velocities, but a combination of the two effects is responsible for the existence of a LL regime at intermediate dopings.

In Sec. VI, we compute spin-correlation functions, which allow us to derive the Knight shifts K and the relaxation rates T_1 for Cu and O nuclei. There are several improved features in our work. In Ref. 23, spin-spin correlation functions were calculated in the low-temperature limit, using Majorana pseudofermions for the spin part. This assumes that gap opening in the spin and in the charge modes occur at well separated T. In bosonization language, spin-spin correlation functions are easily obtained in all cases. For instance, if one treats spin- and charge-density fluctuations on equal footing, one can show that the uniform part of the susceptibility approaches a quantum critical point as doping increases and that at low temperatures in the gapped phase, the staggered part gives a different temperature dependence for each atom in the elementary cell. We also discuss physical implications of the orbital current phase.

II. MODEL

A. Hubbard Hamiltonian for Cu-O two-leg ladders

We consider a two-leg ladder with a unit cell containing two Cu and five O atoms. Two edge oxygen sites are included because they would provide connections with neighboring ladders (which are not considered in the present work).

The Hamiltonian of this system is divided in two parts: the kinetic energy of electrons moving on the lattice H_T (Fig. 1) and electron interactions H_{int},

$$H = H_T + H_{\text{int}}. \tag{1}$$

The explicit form of the first, tight-binding part is

$$\begin{aligned} H_T = \sum_{j\sigma} \Bigg\{ & \sum_{m\in \text{Cu}} \epsilon_{\text{Cu}} n_{mj\sigma} + \sum_{m\in \text{O}} \epsilon_{\text{O}} n_{mj\sigma} \\ & - \sum_{m\in \text{Cu}} t[a^{\dagger}_{mj\sigma}(b_{mj\sigma} + b_{mj-1,\sigma}) + \text{H.c.}] \\ & - \sum_{m\in \text{Cu}} t_{\perp}[a^{\dagger}_{mj\sigma}(b_{m+1,j\sigma} + b_{m-1,j\sigma}) + \text{H.c.}]) \Bigg\} \\ & - \sum_{m=\in \text{O(leg)}} t_{pp}[b^{\dagger}_{mj\sigma}(b_{m+1,j\sigma} + b_{m-1,j\sigma} \end{aligned}$$

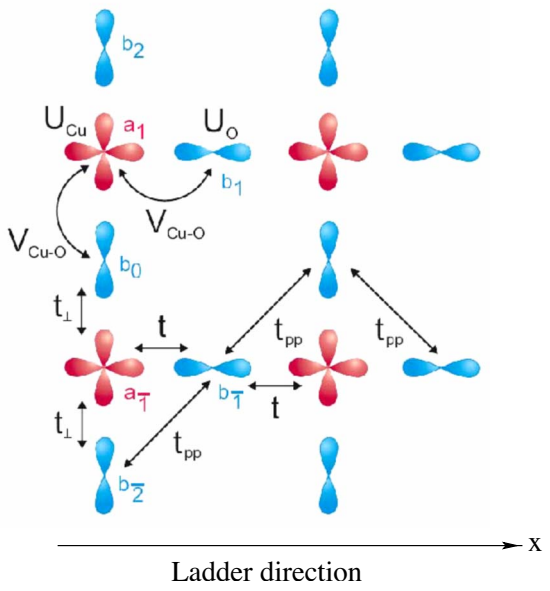

FIG. 1. (Color online) Energy contributions to the Hamiltonian of the Cu-O Hubbard ladder; the figure shows two-unit cells. The subscripts in the a and b annihilation operators track the coordinate of the various atoms in a cell.

$$+ b_{m+1,j-1\sigma} + b_{m-1,j-1\sigma}) + \text{H.c.}]), \tag{2}$$

where $a_{mj\sigma}(b_{mj\sigma})$ annihilates holes with spin σ on a copper (oxygen) site, j labels cells along the chain, and m labels the atoms within each cell. $n_{mj\sigma}=a^{\dagger}_{mj\sigma}a_{mj\sigma}$ is the density of particles on site m, and we use here hole notation such that t, $t_{\perp}$, and t_{pp} are all positive. $\epsilon=\epsilon_{\mathrm{O}}-\epsilon_{\mathrm{Cu}}$ is the difference between the oxygen and copper on-site energies.

The local-density approximation (LDA) determined values[52] of the parameters pertaining to SrCuO systems show that interladder hopping amplitudes are at least *1 order* of magnitude smaller than their intraladder counterparts. Thus the two-leg ladder description is an excellent starting point for these compounds. Inside the elementary cell, t and $t_{\perp}$ are the dominant hoppings and their values are comparable. The difference between the electronic Cu d– and O p–state energies E_{Cu} and E_{O} is about $0.5t$. There do not appear to be *ab initio* determinations of Coulomb terms for SrCuO ladders. However from what is known for cuprates, we may estimate a local U of order $5t$ for the Cu sites, meaning a strongly interacting regime. In the following we will use constant values of the band parameters $t=t_{\perp}=1$ and $\epsilon=0.5$ and treat the other observables (U_{Cu}, t_{pp}/t, $U_{\mathrm{O}}/U_{\mathrm{Cu}}$, and $V_{\mathrm{Cu\text{-}O}}/U_{\mathrm{Cu}}$) as tunable variables. In order to gain insights into the physics of the multiband case, we analyze the above model using a renormalization-group procedure in the interactions; i.e., we assume that all of these are smaller than the kinetic energy. Hence, the validity of the solutions cannot be ascertained in the event when some of the interactions were to grow so large during the flow that they became on the order of the bandwidth. As was stated above, the experimental regime corresponds to a situation where Coulomb terms are sizable. Nevertheless the RG approach allows one to obtain a full analytical solution of this complicated problem and to make detailed comparisons with the physics of the one-band system. Furthermore, for the case of the single-band ladder, one finds that the physical properties in the weakly and strongly interacting limits are smoothly connected. We will come back to that point when we discuss our results.

The eigenvalues and eigenvectors of the noninteracting part are simply obtained by Fourier transforming H_T. Since ϵ is of order t, we neglect the nonbonding and antibonding higher-energy bands which are mostly of p-type character. This reduces the model to two lowest-lying bands crossing the Fermi energy. The Hamiltonian is

$$H_T = \sum_{k\alpha\sigma} e_{\alpha}(k) n_{k\alpha\sigma}, \tag{3}$$

where $\alpha=0,\pi$ denotes the bands and σ are spin indices. The operators corresponding to the eigenstates of H_T are

$$a_{mk\sigma} \ (\text{or} \ b_{mk\sigma}) = \sum_{\alpha} \lambda_{m\alpha} a_{\alpha k\sigma}. \tag{4}$$

$e_{\alpha}(k)$ are the eigenvalues of H_T (the Cu-O distance is set to unity), and $\lambda_{m\alpha}$ are the amplitudes of the overlaps of the eigenvectors with the atomic wave functions in the unit cell. This defines the bonding (o) and antibonding (π) eigenbasis $B_{o\pi}$. For $t_{pp}\neq 0$, the o and π energy bands are the two lowest real solutions of the characteristic equations

$$[\epsilon - e_o(k)][3t_{\perp}^2 + \epsilon^2 - e_o(k)^2] - 2[1+\cos(k)] \times\{-6t_{pp}t_{\perp}t - t^2[\epsilon - e_o(k)] + 3t_{pp}^2[\epsilon + e_o(k)]\} = 0,$$

$$[\epsilon - e_{\pi}(k)][t_{\perp}^2 + \epsilon^2 - e_{\pi}(k)^2] - 2[1+\cos(k)] \times\{-2t_{pp}t_{\perp}t - t^2[\epsilon - e_{\pi}(k)] + t_{pp}^2[\epsilon + e_{\pi}(k)]\} = 0,$$

$$e_o = \epsilon. \tag{5}$$

Including t_{pp} increases the values of the $\lambda_{bi\alpha}$ for the O atoms and makes the o and π bands more asymmetric. However there are still only two bands crossing the Fermi energy, so that the analysis remains valid. We note, however, that the contribution of the oxygen p orbital perpendicular to the one participating in the Cu-O bonding increases as t_{pp} grows larger until, for $t_{pp}>0.5t$, it dominates that of the copper d orbital. Hence, we confine the range of variation of t_{pp} to $0-0.5t$. The interaction part in fermionic language is given by

$$H_{\mathrm{int}} = \sum_j \left(\sum_{m\in\mathrm{Cu}} U_{\mathrm{Cu}} n_{mj\uparrow} n_{mj\downarrow} + \sum_{m\in\mathrm{O}} U_{\mathrm{O}} n_{mj\uparrow} n_{mj\downarrow} + \sum_{m\in\mathrm{Cu}, n\in\mathrm{O}} \sum_{\sigma,\sigma'} V_{\mathrm{Cu\text{-}O}} n_{mj\sigma} n_{nj\sigma'} \right). \tag{6}$$

B. Continuum limit and bosonization

We now express the Hamiltonian in bosonic representation. The procedure is standard[8,53] and we outline only the main steps here. We linearize the dispersion relation in the vicinity of the Fermi energy:

$$H_T = \sum_{|q|<Q} \sum_{r\alpha\sigma} rq V_{F\alpha} a^\dagger_{\alpha rq\sigma} a_{\alpha rq\sigma}. \quad (7)$$

$r = \pm 1$ denotes right and left movers, with momenta close to their respective $\pm k_F$; Q is a momentum cutoff. The boson phase fields denoted by $\phi_{\sigma\alpha}(x)$ are introduced for each fermion specie. $\sigma\alpha$ contains spin and band indices; x is the spatial coordinate along the ladder. Fermionic operators are expressed in terms of the bosonic field $\phi_{\sigma\alpha}(x)$ and $\theta_{\sigma\alpha}(x)$ related to carriers fluctuations by

$$\psi_{r\sigma\alpha} \simeq \eta_{r\sigma\alpha} \exp(\imath k_{F\alpha}) \exp[\imath(r\phi_{\sigma\alpha} - \theta_{\sigma\alpha})], \quad (8)$$

where $\eta_{\sigma\alpha}$ are the Klein factors which satisfy the required anticommutation relations for fermions. These $\eta_{\sigma\alpha}$ do not contain any spatial dependence and they commute with the Hamiltonian operator. They influence only the form of the order operator in bosonic language (through terms of the form $\eta_{\sigma\alpha}\eta_{\sigma\alpha'}$) and the signs of the nonlinear couplings through a Γ coefficient (the eigenvalue of the $\eta_{\sigma\alpha}\eta_{\sigma\alpha'}\eta_{\sigma\alpha''}\eta_{\sigma\alpha'''}$ operator). The operator is unitary so $\Gamma^2 = 1$. This equality applies also to linear combinations of fields (change of basis). Following Ref. 24, we choose $\Gamma = +1$ in the $\sigma+/-$ basis (see below). We also introduce the phase field $\theta_{\sigma\alpha}(x)$; its spatial derivative $\Pi_{\sigma\alpha}(x) = \partial_x \theta_{\sigma\alpha}(x)$ is canonically conjugated to $\phi_{\sigma\alpha}(x)$.

Now the Hamiltonian may be rewritten using the above phase fields. The interaction term in the Hamiltonian can be split into two parts. One part depends only on the density of right and left movers and gives—as does the kinetic energy—a contribution quadratic in the fields ϕ_ν and θ_ν (where ν labels the eigenmodes in the diagonal basis), of the form

$$H_0 = \sum_\nu \int \frac{dx}{2\pi} \left[(u_\nu K_\nu)(\pi \Pi_\nu)^2 + \left(\frac{u_\nu}{K_\nu}\right)(\partial_x \phi_\nu)^2 \right]. \quad (9)$$

For the noninteracting system, one has $K_\nu = 1$ for all modes, and H_0 is quadratic in the diagonal density basis, which is simply $B_{o\pi}$ (the momentum $k_\perp$ associated with the rungs is either 0 or π). Another basis commonly used in the literature is the total/transverse one, B_{+-}. It is related to $B_{o\pi}$ by

$$\phi_{\mu+(-)} = \frac{\phi_{\mu o} \pm \phi_{\mu\pi}}{\sqrt{2}}, \quad (10)$$

where μ stands for spin or charge depending on which density is considered.

In general $\hat{K}$ in Eq. (9) is a matrix, the form of which depends on the basis in which the densities are expressed. For example, if we use $B_{o\pi}$ at the start of the calculation (the basis which diagonalizes the tight-binding part of the Hamiltonian), we obtain

$$\hat{u} \cdot \hat{K}^{-1} = \begin{pmatrix} V_{Fo} & g^{\parallel}_{0\pi} & g^{\perp}_{00} & g^{\perp}_{0\pi} \\ g^{\parallel}_{0\pi} & V_{F\pi} & g^{\perp}_{0\pi} & g^{\perp}_{\pi\pi} \\ g^{\perp}_{00} & g^{\perp}_{0\pi} & V_{Fo} & g^{\parallel}_{0\pi} \\ g^{\perp}_{0\pi} & g^{\perp}_{\pi\pi} & g^{\parallel}_{0\pi} & V_{F\pi} \end{pmatrix} \quad (11)$$

and

$$\hat{u} \cdot \hat{K} = \begin{pmatrix} V_{Fo} & 0 & 0 & 0 \\ 0 & V_{F\pi} & 0 & 0 \\ 0 & 0 & V_{Fo} & 0 \\ 0 & 0 & 0 & V_{F\pi} \end{pmatrix}, \quad (12)$$

where $V_{Fo/\pi}$ are the Fermi velocities in the o and π bands and $g^{\perp(\parallel)}_{ij}$ are interactions between electron densities in the i and j bands, with perpendicular (parallel) spin.

In order to express the Hamiltonian in a Gaussian form [Eq. (9)], which is quite convenient for the RG calculation, we diagonalize $\hat{K}$. This defines the B_o basis. In general, B_o is neither the bonding/antibonding basis $B_{o\pi}$ nor the total/transverse basis B_{+-}. We define the S matrix which describes the relative orientation of the B_o and B_{+-} bases:

$$S = \frac{\sqrt{2}}{2} \begin{pmatrix} P_1 & Q_1 & 0 & 0 \\ -Q_1 & P_1 & 0 & 0 \\ 0 & 0 & P_2 & Q_2 \\ 0 & 0 & -Q_2 & P_2 \end{pmatrix}. \quad (13)$$

One can express the parameters P_i and Q_i with the help of angles α (for the spin part) and β (for the charge part) as follows:

$$P_1 = \cos\alpha + \sin\alpha,$$

$$Q_1 = \cos\alpha - \sin\alpha,$$

$$P_2 = \cos\beta + \sin\beta,$$

$$Q_2 = \cos\beta - \sin\beta. \quad (14)$$

The remaining part of the interactions has a nonlinear cosine form in bosonization language. The most convenient basis to express this contribution is B_{+-} and one finds[8,53]

$$\begin{aligned} H^{\mathrm{NL}}_{\mathrm{int}(1)} = & -g_{1c} \int dr \cos(2\phi_{s+})\cos(2\theta_{c-}) \\ & + g_{1a} \int dr \cos(2\phi_{s+})\cos(2\theta_{s-}) \\ & - g_{2c} \int dr \cos(2\theta_{c-})\cos(2\phi_{s-}) \\ & + g_{4a} \int dr \cos(2\phi_{s-})\cos(2\theta_{s-}) \\ & + g_1 \int dr \cos(2\phi_{s+})\cos(2\phi_{s-}) \\ & + g_2 \int dr \sin(2\phi_{s-})\sin(2\phi_{s+}) \\ & + g_{\parallel c} \int dr \cos(2\theta_{c-})\cos(2\theta_{s-}), \end{aligned} \quad (15)$$

where Γ coefficients determine the signs of the g_i couplings (for instance, this gives minus signs for g_{1c} and g_{2c}). We use the following notation: Indices 1–4 refer to the standard

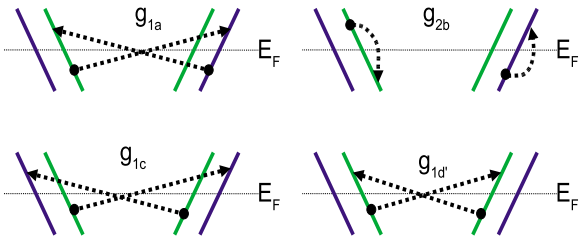

FIG. 2. (Color online) Diagram showing some of the scattering processes. The dark blue (light green) lines are for carriers in the o (π) bands. This illustrates the notation used for the cosine-type terms.

g-ology processes for the left- and right-moving carriers; the letters a–d correspond to similar processes, when the o and π bands labels are used instead of the left or the right labels. The relation between the g_i couplings and the ones in Eq. (6) is given in Appendix A. Note that in the quadratic piece, both g_2- and g_4-type terms need to be included in order to properly account for magnetic fluctuations.[54] Examples of interaction processes are shown in Fig. 2.

For instance, the two g_{1d} terms describe events where one right- and one left-moving fermion, both belonging to the same (0 or π) band, backscatter within that band. If we bosonize this contribution, we find two terms, $g_{1d}\cos(\phi_1+\phi_2)$ and $g_{1d'}\cos(\phi_1-\phi_2)$, instead of $g_{1(2)}$. g_1 and g_2 correspond to the sum of and to the difference between these "1d"-type processes, respectively ($g_1=\frac{g_{1d}+g_{1d'}}{2}$, $g_2=\frac{g_{1d'}-g_{1d}}{2}$); $g_2\neq 0$ when the O atoms are included. If the two bands were equivalent, only the g_1 process would be present.

In a standard Hubbard model, only spin-perpendicular terms are present at bare level, and the last term in Eq. (15) does not appear at the beginning of the flow. However, Nélisse *et al.*[55] pointed out that during the flow toward the fixed point, additional scatterings involving electrons with parallel spins are generated by the RG procedure. In our case, we are including a $V_{\text{Cu-O}}$ term so that right from the start, our model contains interactions between carriers with parallel spin. $V_{\text{Cu-O}}$ gives rise to a nonlinear cosine term, while the other spin-parallel processes, which are generated by the RG procedure, give contributions to the various K.

The g_{4a} term has a nonzero conformal spin and generates two extra couplings during the renormalization:

$$H^{\text{NL}}_{\text{int}(2)} = -G_p\int dr\,\cos(4\phi_{s-}) - G_t\int dr\,\cos(4\theta_{s-}). \quad (16)$$

These additional terms need to be taken into account because they might become relevant when the other interactions scale to zero.

III. RENORMALIZATION-GROUP ANALYSIS

A. Incommensurate filling

We start from the quadratic part of the Hamiltonian and treat the nonquadratic part, Eq. (15), in perturbation, using a renormalization-group procedure. We compute the corrections to the correlation functions to second order in g, and we incorporate them into the LL parameters K. However g terms are expressed in the B_{+-} basis, while the quadratic part, Eq. (9), is diagonal in the B_o basis, so the $P_i(\alpha,\beta)$ and $Q_i(\alpha,\beta)$ coefficients come into play. As a result, off-diagonal terms are generated in the K matrix during the RG iteration. At this stage, B_o is no longer the diagonal basis. In order to fix this, the B_o basis has to rotate during a renormalization cycle. In addition to the standard RG equations for the interactions, we need to find the RG flow of the angles α (for the spin-density basis rotation) and β (for the charge-density basis rotation). So, first we determine the corrections $dK_1,\ldots,dK_4$, dB_{12}, and dB_{34} that change the entries of the K matrix during the initial RG phase. Next, we go back to B_{+-}, using the transformation S^{-1}. Since B_{+-} is a fixed basis, the increments of the K-matrix elements give the RG step corrections expressed in the B_{+-} basis. This new matrix is diagonalized by the operator $S(\alpha+d\alpha,\beta+d\beta)$, where the angles $d\alpha$ and $d\beta$ depend on $dB_{\mu-\mu+}$ and $dK_{\mu-(\mu+)}$ ($\mu=c,s$). The procedure is summarized in the diagram shown in Fig. 3.

A detailed derivation is given in Appendix B, where for the incommensurate case, we set all umklapp terms to zero in Eq. (B16) and we obtain the following set of differential equations

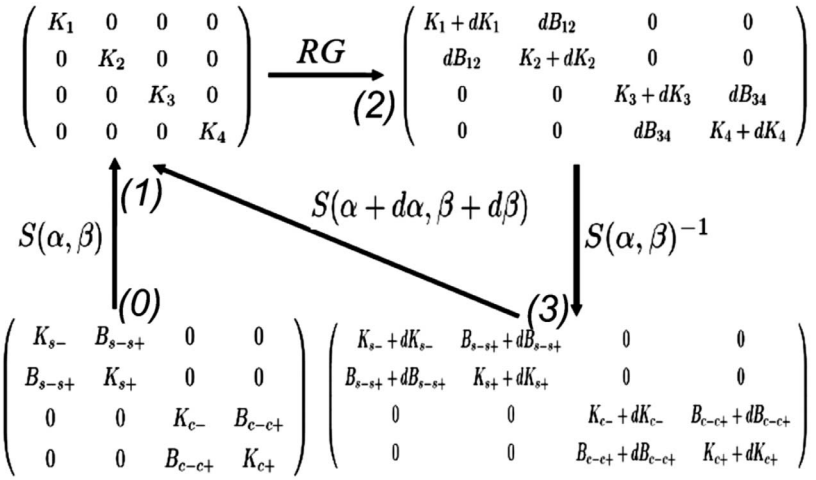

FIG. 3. Diagram showing the flow of the diagonal basis during the renormalization. The bottom row shows the matrix in the fixed B_{+-}. The top row corresponds to the diagonal basis, used to write down the RG equations.

$$\frac{dK_1}{dl} = \frac{1}{2}\Big\{ P_1^2(g_{1a}^2 + g_{\|c}^2 + G_t^2) - K_1^2\Big[Q_1^2 g_{1a}^2 + Q_1^2 g_{1c}^2 + P_1^2 G_p^2 + P_1^2 g_{2c}^2 + \frac{1}{2}(g_1^2 + g_2^2) + f(P_1)(g_1 g_2)\Big]\Big\}, \tag{17}$$

$$\frac{dK_2}{dl} = \frac{1}{2}\Big\{ Q_1^2(g_{1a}^2 + g_{\|c}^2 + G_t^2) - K_2^2\Big[P_1^2 g_{1a}^2 + P_1^2 g_{1c}^2 + Q_1^2 G_p^2 + Q_1^2 g_{2c}^2 + \frac{1}{2}(g_1^2 + g_2^2) - f(P_1)(g_1 g_2)\Big]\Big\}, \tag{18}$$

$$\frac{dK_3}{dl} = \frac{1}{2}P_2^2[g_{1c}^2 + g_{2c}^2 + g_{\|c}^2], \tag{19}$$

$$\frac{dK_4}{dl} = \frac{1}{2}Q_2^2[g_{1c}^2 + g_{2c}^2 + g_{\|c}^2], \tag{20}$$

$$\frac{dg_{1c}}{dl} = g_{1c}[2 - (P_1^2 K_2 + P_2^2 K_3^{-1} + Q_1^2 K_1 + Q_2^2 K_4^{-1})] - (g_1 g_{2c} + g_{1a} g_{\|c}), \tag{21}$$

$$\frac{dg_{1a}}{dl} = g_{1a}\{2 - [P_1^2(K_2 + K_1^{-1}) + Q_1^2(K_1 + K_2^{-1})]\} - g_{1c} g_{\|c}, \tag{22}$$

$$\frac{dg_{2c}}{dl} = g_{2c}[2 - (P_2^2 K_3^{-1} + P_1^2 K_1 + Q_2^2 K_4^{-1} + Q_1^2 K_2)] - g_{1c} g_1, \tag{23}$$

$$\frac{dg_{\|c}}{dl} = g_{\|c}[2 - (P_1^2 K_1^{-1} + Q_1^2 K_2^{-1} + P_2^2 K_3^{-1} + Q_2^2 K_4^{-1})] - g_{1a} g_{1c}, \tag{24}$$

$$\frac{dg_{4a}}{dl} = g_{4a}\Big\{2 - \frac{1}{2}[P_1^2(K_1 + K_1^{-1}) + Q_1^2(K_2 + K_2^{-1})]\Big\}, \tag{25}$$

$$\frac{dg_1}{dl} = g_1[2 - (K_2 + K_1)] + P_1 Q_1(K_2 - K_1) g_2 - \gamma g_{1c} g_{2c}, \tag{26}$$

$$\frac{dg_2}{dl} = -g_2[2 - (K_2 + K_1)] + P_1 Q_1(K_2 - K_1) g_1, \tag{27}$$

$$\frac{dG_p}{dl} = G_p[1 - (P_1^2 K_1 + Q_1^2 K_2)] + g_{4a}^2[P_1^2(K_1 - K_1^{-1}) + Q_1^2(K_2 - K_2^{-1})], \tag{28}$$

$$\frac{dG_t}{dl} = G_t[1 - (P_1^2 K_1^{-1} + Q_1^2 K_2^{-1})] + g_{4a}^2[P_1^2(-K_1 + K_1^{-1}) + Q_1^2(-K_2 + K_2^{-1})]. \tag{29}$$

The equation giving the renormalization of g_2 measures the influence of the O orbitals on the particle-hole asymmetry. The other two are consequences of the g_{4a} term (the term with nonzero conformal spin). Note that we introduced g_1 and g_2—the sum of and the difference between the g_{1d} in both bands—because the renormalization of g_2 involves only g_1 and g_2. The derivation of the renormalization equations in this case is presented in Appendix B. Note also that P and Q depend on α and β [see Eq. (14)], and hence they change during the flow.

Additional renormalization equations for the rotation of B_o are

$$\frac{d\cot 2\alpha}{dl} = \frac{(dK_1 - dK_2)\tan 4\alpha + dB_{12}}{K_1 - K_2} dl^{-1}, \tag{30}$$

$$\frac{d\cot 2\beta}{dl} = \frac{(dK_3 - dK_4)\tan 4\beta + dB_{34}}{K_3 - K_4} dl^{-1}, \tag{31}$$

where the equations for dB_{12} and dB_{34} are

$$\frac{dB_{12}}{dl} = P_1 Q_1[(g_{1a}^2 + g_{\|c}^2 + G_t^2) - K_1 K_2(g_{1a}^2 + g_{1c}^2 + g_{2c}^2 + G_p^2)] - K_1 K_2 h(P_1) g_1 g_2, \tag{32}$$

$$\frac{dB_{34}}{dl} = P_2 Q_2(g_{1c}^2 + g_{2c}^2 + g_{\|c}^2). \tag{33}$$

The function h is defined by

$$h(P_1) = [(P_1 Q_1)^2 + 0.25(P_1^2 - Q_1^2)]^{-1}. \tag{34}$$

As was found in Ref. 16 the interband scattering process (type c) renormalizes the Fermi velocities in both bands to a common value. The additional equation taking this effect into account is

$$\frac{d\gamma}{dl} = \gamma(1 - \gamma)(g_{1c}^2 + g_{2c}^2 + g_{\|c}^2). \tag{35}$$

The initial value of this asymmetry parameter is $\gamma_0 = \frac{1}{2}\tilde{\alpha}^2(\tilde{\alpha} - \frac{1}{2})^{-1}$, where $\tilde{\alpha} = \frac{V_{Fo} + V_{F\pi}}{2V_{Fo}}$. Including this effect does not change our results, but it allows us to determine whether intra- or interband scatterings dominate for a given solution of the RG flow.

If fully spin-isotropic interactions are present in the fermionic Hamiltonian, SU(2) spin-rotational symmetry has to be preserved during the RG flow. Some additional constraints on the RG variables can be derived in this case. For example, one of them (for type-c scattering) is

$$g_{2c} - g_{1c} - g_{\|c} = 0. \tag{36}$$

Rather than using these constraints to reduce the number of RG equations, we check that they are satisfied during the flow.

B. Half filling

If the two-leg ladder is half filled, additional umklapp terms should be included in the Hamiltonian,

$$H_{\mathrm{umk}} = g_{3\parallel}\int dr\,\cos(2\phi_{s+})\cos(2\phi_{c+}+\delta x) + g_{3a}\int dr\,\cos(2\theta_{s-})\cos(2\phi_{c+}+\delta x) + g_{3b}\int dr\,\cos(2\phi_{s-})\cos(2\phi_{c+}+\delta x) + g_{3c}\int dr\,\cos(2\theta_{c-})\cos(2\phi_{c+}+\delta x). \quad (37)$$

Since these terms oscillate with δ, their influence becomes important only for very small doping. The extended system of differential equations describing the RG flow has extra terms compared with the incommensurate case, and each of them is multiplied by a doping dependent coefficient $J_0(\delta)$. The full set of equations is given in Appendix B.

For small δ these Bessel functions $J_0(\delta)$ may be approximated by 1 and for large δ by zero.[33,56] Starting from a small but nonzero doping, assuming that the chemical potential remains constant during the flow, the renormalization equation that describes this Mott physics is[57]

$$\frac{d\delta}{dl} = \delta - (g_{3\parallel}^2 + g_{3a}^2 + g_{3b}^2 + g_{3c}^2)J_1(\delta). \quad (38)$$

The above equation gives an easy way to check if one is in the insulating or in the metallic phase and which set of RG equations (with or without umklapp terms) is valid. $\delta(l)$ flows to zero for the insulator and to infinity for the metal. The value of δ_c depends on the initial values of g_{3i}. The description of this transition is similar to that found in Ref. 33, which focused on the confinement-deconfinement transition of two-chain systems.

For the sake of completeness, let us mention that other types of umklapp terms may appear for the two-leg ladders. These correspond to scattering of electrons in the bonding or antibonding bands, a process which becomes important if one of the k_{Fi} is around $\frac{\pi}{2}$. In the presence of a large $t_\perp$, this condition may be fulfilled for dopings very different from zero. For $t_\perp > 0.1t$ it happens somewhere in the $C2S1$ phase. As was pointed out in the discussion of the incommensurate case, couplings involving θ_{c-} flow then to zero. Thus both in the charge and in the spin sectors, one observes the rotation from the diagonal basis to the $k_\perp = 0/\pi$ basis. There are no processes competing with this, so the only effect is the appearance of a $C1S1$ region inside the $C2S1$ phase. These processes will not be considered in the following.

IV. PHASE DIAGRAM

Using the system of RG equations, we determine the phase diagram. We identify the various phases based on the behavior of the renormalized quantities g_i. We iterate the flow up to a point when some couplings become of order 1. As usual,[8] the bosonized form is very convenient for analyzing the strong-coupling case, since when coefficients in front of cosinelike terms become large, the corresponding variables become locked. Subsequently, one may compute the physical observable in the ground state by looking at the various order parameters in bosonic representation. These operators are given in Appendix C. Some of the operators will now have exponentially decreasing correlations, while others will decay as power laws. The dominant phase is the one for which correlations decrease with the smallest exponent. It corresponds to a quasi-long-range order in the ladder.

Two main factors may significantly affect the phase diagram that was predicted for two-leg Hubbard ladders with a single orbital per site: One is the asymmetry in the g terms due to the fact that the projections of the Cu and O orbitals onto the 0 and π bands have unequal amplitudes and one is the influence of the extra parameters U_{O}, $V_{\mathrm{Cu\text{-}O}}$, and t_{pp}.

We first investigate the impact of the asymmetry by setting $U_{\mathrm{O}} = V_{\mathrm{Cu\text{-}O}} = t_{pp} = 0$ and we choose a small initial value for U_{Cu} (in the range $10^{-6}-10^{-1}$). After this main part we consider a few additional issues such as the spin-rotational symmetry and the stability of the fixed points.

As in Ref. 20 we find that the parameter which describes the behavior of the differential equations system is $\tilde{\alpha} = \frac{V_{Fo}+V_{F\pi}}{2V_{Fo}}$. If the ratio $\frac{t_\perp}{t}$ is constant, $\tilde{\alpha}$ depends only on δ: It is equal to 1 for half filling (then $\delta=0$) and it reaches its maximal value when the Fermi energy is near the bottom of the band. The parameter $\tilde{\alpha}$ is meaningful only if the Fermi energy crosses both bonding and antibonding bands. We restrict our analysis to this case; otherwise one has a single-band LL.

A. Commensurate case

Equations describing the commensurate situation are given in Appendix B 3. In this limit, umklapp terms lead to insulating phases with a gap in the charge degrees of freedom. These states are quite similar to those presented in Ref. 49. In Sec. V B we will discuss this case and also similarities and differences with previous studies.

New and interesting physics occurs when the ladder is doped away from the commensurate case, and we focus on this situation in Secs. IV C and IV E. In the incommensurate case, the asymmetry that is present when the unit cell contains two different atoms (Cu and O) plays a critical role and leads to differences between the single- and multiband models.

B. Small doping case

For small $\tilde{\alpha}$, $\cot 2\alpha \to 0$ and $\cot 2\beta \to 0$, so the total/transverse density basis is the eigenbasis at the fixed point. In this case, g_2, g_{4a}, G_p, and G_t are irrelevant. In the notation of Balents and Fisher,[20] this is the $C1S0$ phase, where only the $c+$ charge mode is massless. Fields θ_{c-} and ϕ_{s+} are ordered with the following values (given mod 2π): $\theta_{c-}=0$ and $\phi_{s+}=0$. For $s-$ the mode (spin-transverse), terms involving both ϕ_{s-} and θ_{s-}, which are canonically conjugated, become relevant, so one observes an ordering competition between these two fields. The analysis of order operators presented in

Appendix B shows that *d*-type superconductivity (SCd) fluctuations dominate if ϕ_{s-} is locked at 0, whereas if $\theta_{s-}=0$ an orbital antiferromagnetic state (OAF) is preferred. In our model, SCd always dominates for repulsive U_{Cu}. This prediction confirms many previous discussions of SCd in two-leg ladders, including in the strong-coupling regime,[29] and in an inhomogeneous doping situation.[58]

The advantage of working in bosonization language is that one can find a reasonable quasiclassical limit of the strong-coupling fixed point. Using a semiclassical approximation for the sine-Gordon model[59] allows one to find the doping dependence of the gaps in the system, which up to now has been obtained only numerically. The following expression for the soliton mass (it is the lowest-lying excitation if $0.5<K_i<2$) is used:

$$m_i = 2\sqrt{\frac{2gu_i}{\pi K_i}}, \tag{39}$$

where u_ν and K_ν are the velocity and LL parameter of the νth mode (by definition we are working in the diagonal basis) and g is the interaction which makes this particular mode massive. For a more detailed discussion of gap evaluation using RG, see, for example, Ref. 60.

The plot shows the behavior of the masses versus doping, evaluated with the above formula. One sees that in the SCd phase, spin gaps go to zero as doping increases and so does the charge-antisymmetric mode, which has the largest value. The behavior of the gaps for small doping, showing a rather slow decay of their values is in agreement with experimental observations.[13] It is also comparable with predictions obtained after refermionization of the problem and mapping it onto an exactly solvable Gross-Neveu model with SO(8) symmetry.[61] (However strict constraints for the Fermi velocities—viz. $V_{Fo}=V_{F\pi}$—and for the ratios of the g couplings at the fixed point have to be fulfilled then.) There were also attempts to reduce the low-energy physics of pure Cu two-leg ladder to an SO(5)-symmetric case.[62,63] For our more general system, these conditions are usually not met. Moreover spurious phases may even appear if one breaks some of the symmetries, so unfortunately we are not allowed to use these integrable models in our calculations. However some predictions, such as the decrease in the gaps with doping and their relative magnitudes, are in complete agreement with these special cases.

It is also worthwhile pointing out that the values of the two spin gaps are always comparable, so that the approximations that are made when $m_1 \gg m_2$ cannot be used here to calculate the physical properties of our model. This behavior pertains to the range $\delta<\delta_{c1}$; upon approaching $\delta_{c1}=0.2$ from below, gaps tend to close. As we will show next, a different phase, *C*2*S*1, emerges for $\delta>\delta_{c2}$. The intermediate range $\delta_{c1}<\delta<\delta_{c2}$ will be discussed separately when we examine the transition from the *C*1*S*0 to the *C*2*S*1 phase.

C. Large doping case

If the asymmetry between the bonding and antibonding bands is larger, $\cot 2\alpha \to \infty$ and $\cot 2\beta \to -\infty$, signaling that $B_{o\pi}$ is the eigenbasis for both the spin and the charge modes. The RG flow converges very quickly to that fixed point for large dopings, typically when $\delta>0.41$. This corresponds to $\tilde{\alpha}=4.2$, a value that agrees with that found previously in Ref. 20. Interactions are not able to renormalize the ratio of the band Fermi velocities γ to 1 anymore, which confirms that the $B_{o\pi}$ basis is relevant for this regime. In the large doping phase, only $g_1 \simeq -g_2$ are relevant. If one takes into account the rotation of the diagonal basis, which occurs as $\cot 2\alpha$ varies, it appears that this flow produces only one massive spin mode, and we get the *C*2*S*1 phase predicted by Balents and Fisher.[20] The interaction term which causes this behavior in our case is identical to theirs once expressed in current-density formalism. Using the same method as the one described for low dopings, we are able to evaluate the doping dependence of the gap of strongly doped ladders. The result is shown in Fig. 5.

One can easily identify the nature of the *C*2*S*1 phase in bosonic field language: Because the diverging interaction is $g_o=g_1-g_2<0$, the slowest decay of correlations is observed for the charge-density-wave (CDW) operator in the bonding ("*o*") band.

For large enough dopings ($\delta>0.41$), a gap will open, even if one starts from very small bare values of the interactions. In the range $0.28<\delta<0.41$, angles still flow to the fixed-point limits $\cot 2\alpha(\beta) \to \infty$, but g_1 and g_2 grow very slowly. One needs to choose larger initial values of the bare interactions (but still smaller than the hopping t) and/or assume that one is close to the *C*2*S*1 region [starting from large $\cot 2\alpha(\beta)$] to find the gap exactly in the relevant spin mode. We conclude that the *C*2*S*1 phase exists in the entire range $\delta>\delta_{c2}=0.28$ and that when $0.28<\delta<0.41$, g_1 and g_2 are very weakly relevant and thus very sensitive to higher-order corrections.

Previously, the existence of a *C*2*S*2 massless phase was predicted very close to the bottom of the band, (i.e., when $\tilde{\alpha}$ becomes quite large). Our calculation, however, shows that the *C*2*S*1 phase remains stable in that limit. The reason for this difference stems from the choice of initial conditions in Ref. 20. For single-orbital ladders, when *only* on-site Hubbard interactions are included, the initial g_2 is accidentally zero. In our case, the presence of O orbitals always implies a nonzero initial g_2. This states that the g_2 term drives the transition for very large $\tilde{\alpha}$.

At the bottom of the band the dispersion is quadratic, so the bosonization procedure, which requires a linear spectrum around the Fermi points, is not valid. The calculation is done using conventional diagrammatic techniques, and it confirms the stability of the *C*2*S*1 phase with the same relevant coupling as found before.

D. Quantum critical regime between the *C*1*S*0 and the *C*2*S*1 phases

We now turn to the intermediate regime $\delta_{c1}<\delta<\delta_{c2}$. Our key finding is that in this range, a massless phase exists, which has not been reported previously because it is found in the asymmetric limit, i.e., when the unit cell contains both Cu and O orbitals.

When one approaches the range $\delta \in (0.2;0.28)$ either from below or from above, gaps appear to go to zero (see

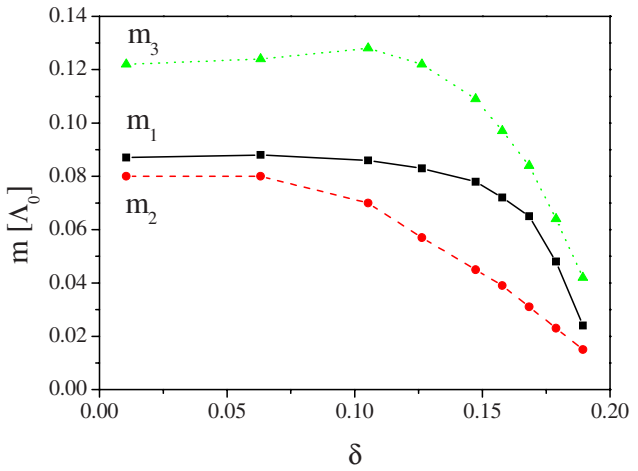

FIG. 4. (Color online) Doping dependence of the gaps in the spin-transverse (1; squares), total (2; circles), and charge-transverse (3; triangles) density modes for the SCd phase. The m_ν are given in units of Λ_0, the initial energy cutoff of the RG procedure (on the order of ~ 1 eV).

Figs. 4 and 5). For $\delta_{c1} < \delta < \delta_{c2}$, one has a line of critical points where the phase is totally massless ($C2S2$). Strong fluctuations, in particular near the critical end points δ_{c1} and δ_{c2}, cause poor convergence of the RG differential equation system. What is more, the angles in Eq. (30) vary significantly in a narrow range of l. Using controlled approximations, we obtain an analytical solution that reveals the behavior of the system in this phase: We approach the critical end points from the massive phases; we keep only the dominant couplings, which gives us a simplified system of equations. Next we analyze the equations describing the angle rotations and look for the range where derivatives become large, which takes place close to the fixed points. This gives us a condition for the divergence of $\cot 2\alpha(\beta)$. Once the fixed point is known, one may simplify further the RG differential system. Now computing the RG exponent of each coupling is straightforward and enables us to find those couplings

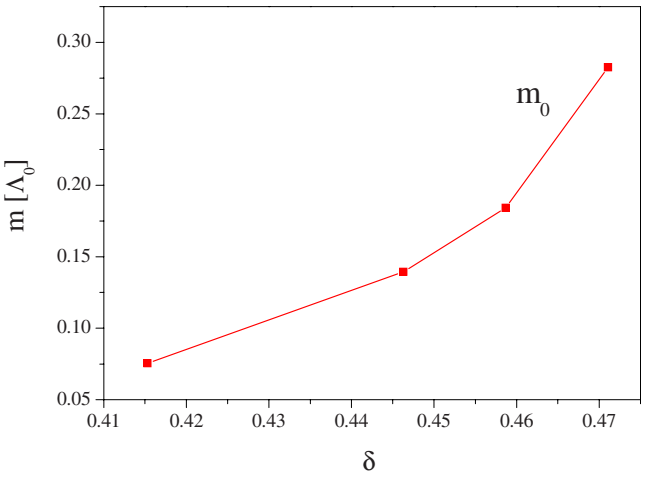

FIG. 5. (Color online) Doping dependence of the gap for the o-band spin mode. Note that the gap is given in units of the cutoff Λ_o, the value of which decreases quickly when one approaches the bottom of the upper band.

which remain relevant within the range of interest.

Let us first consider $\delta_{c2}=0.28$. This point corresponds to the initial value $\cot 2\alpha = 1$. A numerical solution shows that the signs of $(dK_1 - dK_2)$ and B_{12} are the same and positive, whereas the sign of $(K_1 - K_2)$ is negative. From this simple analysis we infer that below this value, $|\cot 2\alpha|$ decreases to zero and that above, it increases to infinity. Now, g_1 and g_2 are relevant only when $(K_2 + K_1) - P_1 Q_1 (K_2 - K_1) < 2$. K_2 needs to decrease strongly for this condition to be fulfilled and it is necessary to have nonzero values of $f(P_1)$ and Q_1 at the fixed point. This condition corresponds to $|\cot 2\alpha| \to \infty$, so one sees that below $\delta_{c2}=0.28$ the g_1 and g_2 couplings cannot be relevant.

The analysis pertaining to $\delta_{c1}=0.2$ is less straightforward. It involves $|\cot 2\beta|$ and, because $(dK_3 - dK_4)$ and B_{34} have opposite signs, it is harder to get the flow correctly. The transition between going to zero and diverging takes place when the absolute value of the two terms are equal. A detailed analysis of the angle dependent part of $d \cot 2\beta$ shows that this happens for $\delta_{c1}=0.2$. When $|\cot 2\beta| \to \infty$, then K_4^{-1}, which is much larger than 1, influences the renormalization of the $\cos \theta_{c-}$ coupling on equal footing with K_3^{-1}. This is the reason why these interactions are not relevant anymore.

The above first-order RG analysis was done in the vicinity of the critical end points and proves that when $\delta \in (0.2; 0.28)$ all interaction terms which are relevant outside are irrelevant inside this range. We have confirmed the above simplified analysis by performing a numerical analysis of the full set of equations, which shows that no other coupling is relevant. We see that a $C2S2$ phase is present between the $C1S0$ and the $C2S1$ phases. Hints for the possible existence of such state came from numerical studies[64] or from some special models of ladders[65,66] with specific types of geometries. However we give here a direct proof of the existence of this phase for a generic ladder.

The $C2S2$ phase is a LL where $B_{o\pi}$ is the fixed-point eigenbasis for the charge modes and B_{+-} that for the spin modes. As far as the charge modes are concerned, $K_{4\equiv o}$ is significantly smaller than 1, while $K_{3\equiv\pi}$ is very close to 1 at the fixed point. The spin parameters are both close to 1 because of the spin-rotational symmetry. Thus one expects that correlation functions of band-density fluctuations of the form $c^\dagger_{+/-,o}\sigma_i c_{+/-,o}$ have the slowest decay. Logarithmic corrections need to be evaluated, owing to the presence of a (single) marginal coupling $g_o = g_1 - g_2 > 0$. They show that a spin-density wave (SDW) within the o *band* [SDW(o)] is dominant.

E. Influence of U_O and $V_{Cu\text{-}O}$

So far, we have discussed only changes that stem from the presence of O orbitals in the structure. We now turn on the interactions involving the O atoms—U_O and/or $V_{Cu\text{-}O}$—and probe whether these additional terms affect or not the phase diagram that we have found previously. In the following, we assume that these interactions do not generate new types of terms in bosonization language but that they modify the initial parameters of the flow. (For a detailed discussion of V-type terms, see, for example, Ref. 67.)

In the $C1S0$ phase, SCd becomes less stable if large U_O or $V_{Cu\text{-}O}$ are present, but it always has a lower free energy than that of the OAF phase. When both U_O and $V_{Cu\text{-}O}$ are present, they seem to have competing effects. One would need to assume a very large attractive bare $V_{Cu\text{-}O}$ ($V_{Cu\text{-}O}<-3.6U_{Cu}$) in order to stabilize a phase different from SCd. It would be an s-type superconductivity (SCs) phase with $\phi_{s-}=0$, $\phi_{s+}=0$, and $\theta_{c-}=\pi/2$ and it would be very robust, even if the Fermi level approaches the bottom of the π band. The existence of this phase, generated by $V_{Cu\text{-}O}$, was first pointed out in Ref. 49. The discussion in Ref. 49 pertains to the half-filled case. The nature of the phase transition between the two superconducting phases in ladders is described in detail in Ref. 24, so we are not going to discuss this point. In the physical range of values of bare $V_{Cu\text{-}O}$, one does not expect SCs to dominate.

In the $C2S1$ phase, U_O and $V_{Cu\text{-}O}$ do not change the results significantly. Their main influence is that they make the gap smaller. It is to be expected, since the CDW in the o band has an overlap with O atoms sitting between two Cu and introducing electron repulsion on O atoms makes the CDW less stable. For very large attractive $V_{Cu\text{-}O}$, the SCs phase re-enters.

In the $C2S2$ phase, increasing $V_{Cu\text{-}O}$ has little effect on δ_{c2} but it shifts δ_{c1} to higher values. For $\frac{V_{Cu\text{-}O}}{U_{Cu}}>1$ the quantum critical line still exists and an unphysically large ratio of ≈ 5 would be required to suppress the massless phase and to observe a re-entrant $C1S0$ phase with superconducting fluctuations. The δ_{c1} phase boundary is not affected by U_O or by $V_{Cu\text{-}O}$.

V. DISCUSSION AND CONSEQUENCES

In this section, we discuss our findings in connection with previous work done on ladders. We also show that the $C2S2$ and $C2S1$ phases possess an orbital current quasi-long-range order and we compare our result with other proposals of current patterns for cuprates.

A. Differences with the single-band case

In the derivation of the RG equations using current algebra, total particle-hole symmetry was assumed. Yet, it was shown[68] that V-type interactions, for instance, can generate terms which break this symmetry at the beginning of the flow. They generate the following terms:

(a) A sine interaction term, $g_2 \sim g_{1o}^{\perp}-g_{1\pi}^{\perp}$.

(b) Interactions such as $g_{2o}^{\perp}-g_{2\pi}^{\perp}$ and $g_{1o}^{\parallel}-g_{1\pi}^{\parallel}$, of the form $\nabla\phi_{s+}\nabla\phi_{s-}$, which are included in the definition of the non-diagonal part of the $\hat{K}$ matrix [see Eq. (9)]. This implies, for instance, that $P_1 \neq P_2$.

(c) g_4-type interactions, which generate different velocities for the spin and charge modes. (*Per se* this is not a relevant perturbation but it enhances the impact of the other two contributions.)

When O atoms are included between Cu atoms, even if *only* U_{Cu} is present, the bare $g_0 \sim \frac{\lambda_{ao}^4}{V_{Fo}}U_{Cu}$ is different from $g_\pi \sim \frac{\lambda_{a\pi}^4}{V_{F\pi}}U_{Cu}$ and particle-hole symmetry does not hold anymore. [In the limit $E\to\infty$, one has $\lambda_{ao}^4-\lambda_{a\pi}^4 \sim E^{-1}$ and $V_F \sim E^{-1}$ so these two effects cancels out and g_o-g_π is still $\sim O(1)$]. This shows that it is quite important to include the oxygen atoms in the description of the two-leg ladder.

The system of RG equations that we have derived does not impose such particle-hole symmetry constraint. Hence it may flow to a new fixed point which corresponds to the $C2S2$ phase. At the fixed point, B_{+-} is the diagonal basis for the spin modes and $B_{o\pi}$ is the diagonal basis for the charge modes. It should be emphasized that for all other phases (which have been found previously for single-orbital ladders), initial conditions which reflect the symmetries of the problem impose that the diagonal basis at the fixed point be the same for the spin and for the charge modes. The presence of the three bands thus allows the symmetry between spin and charge bases to be relaxed during the flow and is instrumental in stabilizing the $C2S2$ phase. For the case of a single band, Emery *et al.*[69] pointed out that two additional considerations could lead to a significant modification of the phase diagram obtained in Ref. 20, using a weak-coupling perturbative approach. The first one was the inclusion of all interactions, not simply the relevant ones; the second one was the stability of the fixed points. For example, in Ref. 69, it was argued that the stability of the $C2S1$ phase was compromised because of a "spin proximity effect." However this $C2S1$ phase was found in DMRG numerical studies.[70] In our calculation it is important to note that all possible interactions were taken into account, and we did not impose any *a priori* symmetry. The presence of the $C2S1$ phase, which we do find in our calculation, is thus intimately connected with the rotation of the spin basis toward the fixed-point $B_{o\pi}$ eigenbasis.

As we argue now, performing a rotation of the eigenbasis, however complicated as it may seem at first sight, is the proper way to implement the RG procedure for all dopings. The bosonic representation is convenient for handling the $C1S0$ phase, and let us assume that we work within the fixed B_{+-} basis. Far away from half filling (for instance, near δ_{c1}), the quadratic part of the Hamiltonian exhibits "significantly large" off-diagonal terms at the start of the flow. However, since B_{+-} is the fixed-point eigenbasis, these contributions eventually go to zero at the end of the RG process. The evolution is beyond the regime where perturbative calculations are reliable. Importantly, this will happen while interactions renormalize so we will not have any information about the physical nature of the ground state in this case. For $\delta>\delta_{c2}$, $B_{o\pi}$ is the fixed-point eigenbasis; hence, fermionic g-ology,[16] where one uses the $B_{o\pi}$ representation, is well suited for studying the $C2S1$ regime. However, the $C2S2$ phase lies beyond the limit of perturbative analysis in that language. One would observe the divergence of some fermionic couplings, while some nontrivial combination of them would remain quite small. By contrast, for all dopings, our approach amounts to adjusting the basis in such a way as to remain in the weak-coupling regime of the off-diagonal elements of the K matrix during the entire flow. It allows us to track the evolution with doping of massive phases into a massless phase as a result of a symmetry breaking (the eigenbasis for the spin and the charge modes) due to the oxygen atoms.

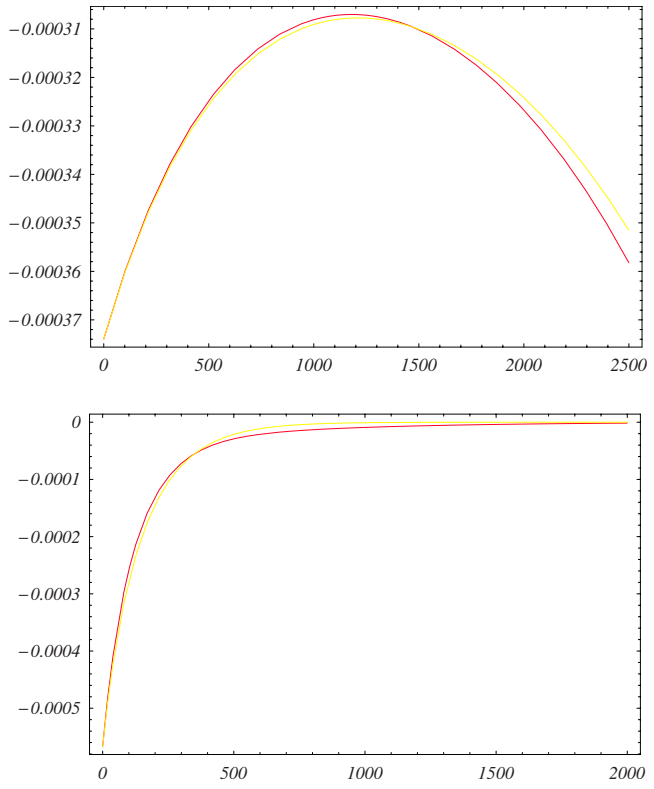

FIG. 6. (Color online) Evolution of g_{2c} (light yellow line) and $g_{1c}+g_{\|c}$ (dark red line) versus number of RG steps during the flow. This figure shows that spin-rotational symmetry is preserved: (a) small α phase; (b) large α phase.

At each step, we monitored the spin-rotational invariance of the Hamiltonian through Eq. (36) to check that our equations were producing a reliable flow. The result for the case of small as well as large dopings is displayed in Fig. 6.

In addition, in the $C2S1$ phase, there is one single massless spin mode, so that its K parameter must remain equal to 1 during the flow. We verified that this property does hold.

B. Half filling and close to half filling

At half filling, the charge-symmetric mode becomes massive. All modes are gapped and spatial correlations decay exponentially. This is due to three relevant umklapp couplings. The spin- and charge-transverse modes are locked into the same minima as before, and the transition affects only the total charge mode. One may view this transition as a quantum order-disorder Ising type. At half filling the dominant phase is the quantum disordered D-Mott phase, which, upon doping, turns into SCd, its dual counterpart. For large attractive V, an S-Mott phase, the dual counterpart of SCs, dominates at half filling. When we vary the strength of the interactions, the boundaries between these two phases look similar to those found for incommensurate fillings.

The half-filled case for the Cu-O ladder was discussed by Lee *et al.*,[49] both in the weak- and in the strong-coupling limits. For weak interactions, we may directly compare their results with ours. They used current algebra to treat the low-energy physics of ladders with and without outer oxygens (five and seven atoms in the unit cell, respectively). In the latter case, a spin-Peierls bond-density wave (BDW) (see Appendix C) dominates, whereas a D-Mott phase is favored in the former case. The authors claimed that this difference is due to a larger leg to rung anisotropy when outer oxygens are not present. The outer oxygens were taken into account in our model but we nevertheless find a D-Mott phase. More generally, our entire phase diagram is very similar to their "five-orbital" case. A possible reason for this discrepancy could be that their t_{pp} is barely less than the Cu-O hopping amplitudes. In our calculations t_{pp} is much smaller, in accordance with LDA studies[52] and with experiments. Recall that, as was described in Sec. II, whenever $t_{pp}>0.5t$ (or $t_{\perp}$), nonbonding p orbitals become relevant degrees of freedom; these were not included in our model. Similarly a large initial value of the nearest-neighbor interaction V causes an exchange of the weights of the d and p orbitals in the lowest-lying bands during the RG flow. This limit is beyond the range of validity of a simple RG approach.

The strong-coupling case (the so-called charge-transfer regime) is important because, for real inorganic materials, U is usually of order $5t$. Still, two features of the weak-coupling regime remain valid in strong coupling: One is that spin-charge separation holds and the other is that in the SCd phase (for instance) there is still an exponential decay of DW operators. A connection between the phase diagrams of these two regimes is often suggested in the literature. For instance, in the case of Cu-O ladders close to half filling (the strong-coupling case discussion in Ref. 49), a t-J approximation was used. It gave a uniform phase—related to D-Mott—in a broad region of positive U_{Cu}-$V_{\mathrm{Cu\text{-}O}}$ phase space. For large attractive $V_{\mathrm{Cu\text{-}O}}$, a phase with holes localized around copper atoms is found, probably connected to our SCs ordering. Our phase diagram matches the above description. The SCd phase, which we find close to half filling, is clearly seen in numerical studies. The $C1S0$ phase was connected with this type of ordering in Ref. 29, where it was also shown that the gap preventing a DW-type ordering decreases upon increasing the doping. In Ref. 71 it was found that the region where this phase is stable can be extended up to $U=4t$. In the t-J model, the rigidity of SCd with respect to a finite difference between the chemical potentials of the two legs was also established.[58] The same type of ordering (rung singlet) also dominates at half filling for a special choice of parameters giving an SO(5) symmetry,[72] since in that case one may solve the model exactly. All these results were obtained for single-band ladders. Quantitative differences occur when oxygen atoms are included in the unit cell, and these were analyzed in a numerical study.[50]

A few studies were devoted to the intermediate and large doping regimes. We discussed the $C2S1$ phase (see above), and as far as the $C2S2$ phase is concerned, a DMRG study[64] suggested the existence of such gapless phase well inside the bands for a zigzag ladder. The occurrence of a massless phase in the strong-interaction limit would be certainly remarkable.

C. Orbital current patterns at intermediate and large dopings

In Secs. IV, V A, and V B, we had set $t_{pp}=0$. We now assess the influence of this hopping term on the phase dia-

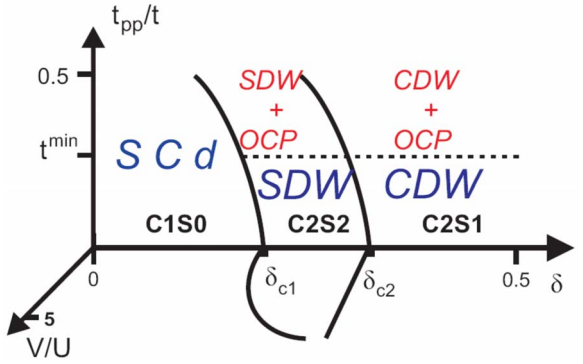

FIG. 7. (Color online) Phase diagram of two-leg Hubbard ladders versus doping for $U_{Cu}>0$. $\delta=0$ corresponds to the half-filled case; umklapp terms which open up a gap in the charge-symmetric mode are not included here. DW+OCP denotes phases with OCP on top of a SDW or a CDW.

gram. As long as $t_{pp}<0.5t$, our RG method remains valid, and only the initial parameters change with t_{pp}. As we increase t_{pp}, we note that $\tilde{\alpha}$ increases for a given doping, but that both δ_{c1} and δ_{c2} are decreasing. For $t_{pp}=0.5$, their values are about half of that quoted for $t_{pp}=0$. A negative t_{pp} (the electron-doped case) has the opposite effect. This influence of $t_{pp}>0$ can be understood as an increased asymmetry between bands.

The phase diagram, which summarizes our study of the Cu-O ladder for carrier concentrations between half filling down to the bottom of the "upper" band, is shown in Fig. 7. A spectacular effect of t_{pp} is that it leads to new types of current loops, involving oxygen sites. The range of parameters where orbital current patterns (OCPs) dominate is seen in Fig. 7.

A finite t_{pp} allows direct current flows between oxygen atoms, giving rise to additional patterns, enclosed inside the elementary cell. One of these preserves the mirror symmetry on the σ axis (the axis parallel to the chain direction and passing through the midrung oxygens), and it is of special importance. This is because we have shown that, at least for moderate dopings, operators in the o band dominate. The current operator between two atoms "a" and "b" is defined as $j_{a\text{-}b}=\Sigma_{\alpha,\alpha'}\psi^{\dagger}_{\alpha a}\psi_{\alpha' b}-\psi^{\dagger}_{\alpha' b}\psi_{\alpha a}$ (we sum over band indices) and the total current pattern operator is given as a sum of currents on each bond. For symmetry reasons, if the current pattern has a mirror symmetry along σ, then the total current operator has the form of a particle-hole fluctuation in the o band.

Two conditions must be met in order to get a dominant contribution: The pattern must form closed loops originating from and ending at Cu atoms, and it has to possess a mirror symmetry with respect to the plane containing σ and perpendicular to the plane of the ladder. One of the current patterns preserves both of the required constraints and, since it is similar to a configuration proposed by Varma, we call it *"VarmaI" type* (Fig. 8). Then, because the current operator has the same dependence on phase fields as the DW operator, these fluctuations have the same power-law decay. Computing their amplitude will tell us which type of order dominates.

In the large doping regime ($C2S1$), we compare the amplitudes of the "normal" CDW and of the OCP+CDW. The

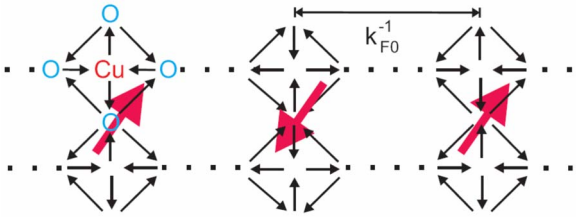

FIG. 8. (Color online) Current pattern in the $C2S2$ phase. It has a mirror symmetry with respect to the σ axis plus an additional SDW. The modulation has an incommensurate spatial periodicity $2k_{F0}^{-1}$.

amplitude of the latter is found by summing current operator contributions for loops with one Cu and two O atoms. We use the mirror symmetry and add first equivalent pairs of currents. Each of these pairs gives a contribution proportional to $t_{ij}\,\mathrm{Im}(\lambda_{a\alpha}\lambda_{bi\alpha})$ or $t_{ij}\,\mathrm{Im}(\lambda_{bj\alpha}\lambda_{bi\alpha})$, where t_{ij} is the hopping parameter between the relevant atoms. We emphasize once again that in the single (Cu)–orbital case, $\lambda_{a\alpha}=1$ so that the current operator between Cu atoms has the usual interband form. It is the presence of oxygens that gives $\mathrm{Im}(\lambda_{a\alpha}\lambda_{bi\alpha})\neq 0$, allowing the geometry of a Varma-type pattern to appear in the theory.

A numerical calculation shows that these quantities are of order 1 and change only by a few percent when the doping increases from 0.25 to the value of δ at the bottom of the band. The result of this procedure (the amplitudes of the currents determined by the products of λ_{ij} coefficients) is shown in Fig. 9. Since it is easier to visualize a commensurate pattern, we chose $\delta=0.9$ such that $k_{Fo}=1/4$ (note that only the "0" band would cross the Fermi level for such a large value of the doping).

Due to current conservation, the weakest link between atoms determines the maximum value of the current. It is clear that the magnitude of t_{pp} determines whether or not the OCP+CDW state may exist. Since the total amplitude is proportional to $2t_{pp}\Sigma_{ij}\mathrm{Im}(\lambda_{bj\alpha}\lambda_{bi\alpha})$ multiplied by the number of links, it is straightforward to obtain a threshold value of $t_{pp}^{(\min)}\approx 0.3t$, above which the OCP+CDW phase dominates.

Varma's work was concerned with the strong-coupling regime in two dimensions, and the stability of the current patterns was studied in mean-field theory. The fact that we were able to find such a state in one dimension, in the weak-coupling limit and with purely repulsive interactions, gives an interesting perspective on the possible existence of such orbital currents. Note that a type of ordering similar to the one we find (current+DW) has been suggested in numerical studies of two-leg ladders.[30,44] We will return to this issue in Sec. V D, where we make a contact with strong-coupling results. The statement about the existence of OCP states given above obviously holds also for the $C2S2$ phase, where CDW fluctuations are replaced by SDW fluctuations (Fig. 8). We also note two differences between our orbital current states and Varma's: In our case, the structure is incommensurate (the modulation is doping dependent) and we get an additional DW modulation. Hence, the OCP+DW state also share similarities with the DDW phase.[46] The main point is that introducing t_{pp} gives the possibility of having new types of current loops involving oxygen sites. Phases with time-

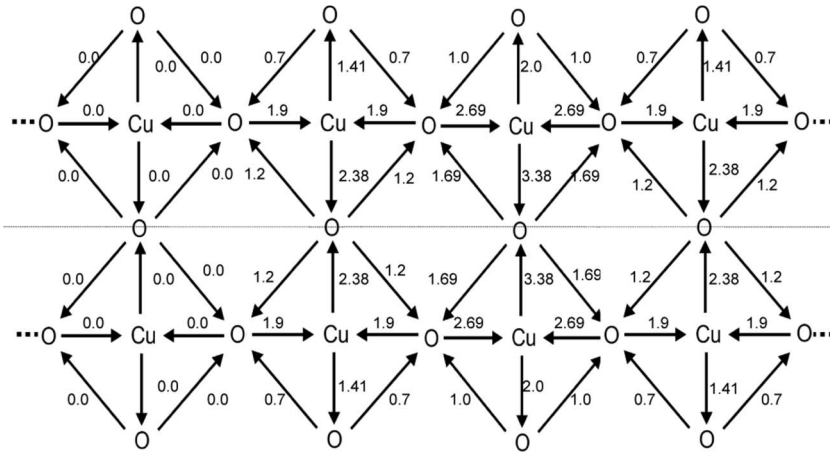

FIG. 9. Current amplitudes within the o band, given in t_{pp} units. For this particular doping, the pattern has an eight-cell periodicity. The figure shows half a period (the other half is simply obtained by repeating the amplitude pattern and reversing all the signs).

reversal symmetry breaking have been widely investigated, but for single-orbital models, currents flow along Cu square plaquettes, giving rise to the OAF state. As was shown in detail by Fjærestad and Marston,[73] these are described by interband creation-annihilation process $\sim\psi_o^\dagger\psi_\pi$. The order operator in bosonization language is given in Appendix D [it is the $O_{\hat{OAF}}(r)$ operator] and, this type of quasi-long-range order is stable *provided* one introduces an attractive $V_{\text{Cu-Cu}}$.

What about current patterns in the strong-coupling regime? This issue was investigated numerically. One paper[30] showed that if time-reversal symmetry is artificially broken by adding a magnetic field, one promotes a state with OAF currents and a CDW modulation for the two-leg ladder, very similar to the one suggested in Sec. IV. Another[44] considered variants of t-J models, in hopes of finding current pattern phases. Although somewhat artificial values were assigned to some of the parameters, this study suggested that quasi-long-range order of the current patterns could be obtained provided one changed the internal description of the rung. Furthermore, the current pattern is accompanied by a charge-density-wave structure.

It should be pointed out that both papers established a direct connection between the strong- and the weak-coupling regimes. For example, Ref. 44 showed that the spatial decay of current-current correlations is similar in regions of parameter space corresponding to weak- or large-coupling RG. This paper also emphasized that in order to obtain current patterns, one needs to go beyond theories using properties of SO(5)-symmetric models. This confirms our findings that new physics emerges in formalisms where symmetry breaking is *a priori* allowed.

D. Experimental systems

Experimentally, it is rather difficult to vary the doping in ladder compounds, and the large doping regime is still inaccessible.[74] Furthermore, different methods (NMR, optical conductivity, and x-ray measurements) yield different values of the doping for a given system.[75] One of the most interesting compounds, $Sr_{14-x}Ca_xCu_{24}O_{41}$, contains both chains and ladders, and it was shown that a change in pressure may cause a charge transfer between the two.[9] Calcium is also a factor that affects the carrier content of the ladder. In the low doping regime, this system displays spin gaps, as is well established in many NMR studies; this will be discussed in detail in Sec. VI. As far as charge degrees of freedom are concerned, the situation is more complicated. There are optical conductivity measurements showing CDW ordering in these systems at ambient pressure.[76] This kind of ordering may be due to a large $V_{\text{Cu-Cu}}$ (Ref. 77) not taken into account in our model or to interladder electrostatic interactions. The SCd phase appears under pressure, with a maximum temperature on the order of 10 K for an optimal pressure of 3.5 GPa. The role of pressure in this transition is not clear: It may change the bandwidth, the couplings between ladders, the screening of the intra- or interladder interactions, or the doping. Recently,[78,79] soft-x-ray measurements were performed for this system. The main conclusion is that an insulating "hole crystal" phase exists for commensurate fillings. It is suggested that this phase melts for other dopings. The authors of these papers interpreted their findings by invoking strong on-rung hole pairing. This analysis supports the picture that emerges from our study of the low doping regime.

VI. NMR PROPERTIES

A. Spin susceptibility and NMR relaxation rate

The spin operator with momentum q is defined as

$$S_m^i(\mathbf{q}) \equiv \frac{1}{2}\sum_{\mathbf{k}\sigma 1\sigma 2} c_{m\sigma 1}^\dagger(\mathbf{k}+\mathbf{q})\hat{\sigma^i}c_{m\sigma 2}(\mathbf{k}), \tag{40}$$

where $c \equiv a,b$ (the annihilation operator of a hole on Cu or on O, respectively) and $\hat{\sigma^i}$ is a Pauli matrix. From linear-response theory, the time-ordered susceptibility reads

$$\chi_{m'm}^i(\mathbf{q},\iota\omega_n) \equiv \frac{1}{2L}\int_0^\beta d\tau\langle T_\tau S_{m'}^i(\mathbf{q},\tau)S_m^i(-\mathbf{q},0)\rangle\exp(\iota\omega_n\tau). \tag{41}$$

The above function is defined only for Matsubara frequencies ω_n. Taking the analytical continuation, one obtains the retarded susceptibility $\chi_{m'm}^R$ (Ref. 8) and hence derive[53] analytical expressions for the measured NMR properties of the system. The NMR signal comes from a contact interaction

between a nucleus and the surrounding cloud of electrons in an *s*-orbital state.

The temperature dependence of the shift in (Zeeman) frequency of the *m*th nucleus stems from hoppings of carriers from the *m*th atom *s* orbital to the highest occupied molecular orbital *p* or *d* orbital of the neighboring sites. Thus, the Knight shift is

$$\bar{K}_m^i = \frac{C_m}{\gamma_m \gamma_e \hbar^2} \sum_{m'} \chi_{m'm}^{Ri}(\mathbf{p} \to 0, \omega = 0), \tag{42}$$

where the summation is taken over all neighboring Cu *d* and O *p* orbitals. The overlap coefficients $\tilde{\lambda}_{m\alpha}$, which enter $\chi_{m,m'}$, are evaluated using first-order perturbation theory. We include hoppings between a Cu *s* orbital and an O *p* orbital on the neighbor sites or a Cu *d* orbital on next-nearest-neighbor sites, as well as hoppings between an O *s* orbital and a Cu *d* orbital on neighboring sites.

The spin-lattice relaxation rate is also affected by the electronic environment. The signal measured on the *m*th nucleus is given by

$$\left(\frac{1}{T_{1m}}\right)^i = \frac{C_m^2}{\gamma_m \gamma_e \hbar^2 \beta} \sum_{\mathbf{p}} \frac{\mathrm{Im}[\chi_{mm}^{Ri}(\mathbf{q}, \omega_{Zm})]}{\omega_{Zm}}. \tag{43}$$

In the following, we omit the "*i*" subscripts because we are working with spin-rotational invariant models. Taking into account the fact that the Fermi surface consists of pairs of points of the form $\pm k_F$, the sum in $\frac{1}{T_1}$ can be divided into two independent parts: a uniform piece (**q** around $k_\parallel = 0$) and a staggered piece (**q** around $k_\parallel = 2k_F$).

Using the $\tilde{\lambda}_{m\alpha}$ allows us to connect the time-ordered correlation functions $R_\alpha(r(x,\tau))$ of carriers in band α (they are introduced in the bosonic phase field language), with the $R_{m'm}(r(x,\tau))$ defined for a site basis as

$$R_{m'm}(r(x,\tau)) = |\tilde{\lambda}_{m'o}|^2 |\tilde{\lambda}_{mo}|^2 R_o(r(x,\tau)) + |\tilde{\lambda}_{m'\pi}|^2 |\tilde{\lambda}_{m\pi}|^2 R_\pi(r(x,\tau)). \tag{44}$$

In order to get the retarded $\chi_{m,m'}^R(q,\omega)$ entering Eqs. (42) and (43), we use the fact that correlations for spin operators and for their complex conjugates are equal, and we simply obtain the retarded spin susceptibility by a Wick rotation,[80]

$$\chi_{m'm}^{Ri}(x,t) = 2\theta(t)\mathrm{Im}[R_{m'm}(r(x,\tau))]_{\tau = it+\delta}, \tag{45}$$

followed by Fourier transforming the last function.

Because of conformal symmetry in our 1D quantum theory, results for zero-temperature correlations can be extended to finite temperatures by simply substituting for the complex coordinates the following expression:

$$r_\nu(x,\tau,\beta) = \frac{u_\nu \beta}{\pi} \sqrt{\sinh\left(\frac{x - \imath u_\nu \tau}{\frac{u_\nu \beta}{\pi}}\right) \sinh\left(\frac{x + \imath u_\nu \tau}{\frac{u_\nu \beta}{\pi}}\right)}. \tag{46}$$

The substitution $r_\nu(x,\tau) \to r_\nu(x,\tau,\beta)$ gives us the temperature dependence of the susceptibilities. This procedure is valid both for the uniform and for the staggered parts of the magnetization. We write the time-ordered correlation functions $R_\alpha(r(x,\tau))$ in each band in terms of diagonal modes $R_\nu(r(x,\tau)) = F[\phi_\nu]$ for the staggered and the uniform parts, separately. The form of $F[\phi_\nu]$ depends on whether the νth LL mode is massless or massive and it will be presented below. Given $F[\phi_\nu]$, substitution (46) allows us to obtain the temperature dependence of K_m and T_{1m}^{-1}. However as the temperature increases, the form of $F[\phi_\nu]$ changes. Generally it is assumed that above the temperature T_ν corresponding to the value of the gap Δ_ν, thermal fluctuations make the νth mode massless. For example, at $T=0$, in the $C1S0$ phase, one starts with three gapped modes (two for the spin and one for the charge). We increase T until the energy of the first gap, Δ_{s+}, is reached. Above the corresponding temperature T_{s+}, we may consider that there is effectively one gapped and one gapless spin mode and similarly for the charge sector. The others gaps (Δ_{s-} and Δ_{c-}) will successively close at temperatures T_{s-} and T_{c-}.

B. Doping dependence of the NMR signals

A number of papers[81–83] were devoted to the computation of magnetic properties of two-leg ladders by assuming symmetry entanglement at the fixed point [SO(5) or SO(8)]. Yet, following the discussion in Sec. IV, we use simpler, approximate methods which nevertheless have a wider range of validity.

1. Uniform part

For the uniform magnetization, only spin correlations need to be taken into account. Because the spin density is generally related to the spin phase field $\sigma(x) = \frac{1}{\pi} \nabla \phi_\sigma(x)$, the zero-momentum part of $\bar{R}_o$ is a linear combination of bosonic correlations calculated in the diagonal basis $\bar{R}_\nu(r)$. In the massless case it is known from LL properties and given by

$$\bar{R}_\nu = \frac{1}{r_i^2}. \tag{47}$$

The contribution to NMR of these power laws has been evaluated many times before in the literature. One gets a T^0 dependence for the Knight shift and T^1 for the relaxation rate. One may improve these results in both the high- and the low-energy limits. At low energies, logarithmic corrections from relevant and marginal couplings $g(\Lambda)$ (where the energy scale Λ may be related to the temperature) should be taken into account. Then, g_{1c} and g_{2c} contribute to the o and π bands, $g_1 - g_2$ to the o band, and $g_1 + g_2$ to the π band. At high energies, the curvature of the bands may be taken into account using a random-phase approximation (RPA), following Refs. 23 and 84.

In the massive case we use the massive Gaussian model to obtain fluctuations around the static quasiclassical solution (equilibrium position) and this leads to

$$\bar{R}_\nu = K_i[\kappa_0(m_i r_i) + \kappa_2(m_i r_i)], \tag{48}$$

where we have used the fact that for harmonic fluctuations around the soliton $\delta\phi_i(x) \equiv \phi_i(x) - \phi_{oi}(x)$, correlations are given by a Bessel function $\langle \delta\phi_i(r)\delta\phi_i(0)\rangle \simeq \kappa_0(m_i r)$. A first-order expansion, valid for large r, gives exactly the same expression as that found in exact calculations.[85,86] One needs to evaluate the following integrals [the exact formulas for the LL $\chi(k,\omega)$ are known[87] but it is not necessary to use them here]:

$$\frac{1}{T_{1m}} = \int dt \sum_{x_0} F[\widetilde{\lambda_{m\nu}}^2(x_0)]R(x_0,t), \tag{49}$$

$$\bar{K}_m = \widetilde{\lambda_{m\nu}}^2(k=0)\left[\sum_{m'} \widetilde{\lambda_{m\nu}}^2(k=0)\right]\int dtdxR(x,t), \tag{50}$$

where the summation over x_0 accounts for the momentum dependence of $\widetilde{\lambda_{m\nu}}(k)$. For the uniform part, integrals can be calculated analytically,

$$\frac{K_i m_i V_i}{\pi}\kappa_0(m_i r_i)\frac{\cosh\left[\frac{\pi(x-\imath V_i t)}{V_i\beta}\right]\sinh\left[\frac{\pi(x+\imath V_i t)}{V_i\beta}\right] - \sinh\left[\frac{\pi(x-\imath V_i t)}{V_i\beta}\right]\cosh\left[\frac{\pi(x+\imath V_i t)}{V_i\beta}\right]}{\sqrt{\sinh\left[\frac{\pi(x-\imath V_i t)}{V_i\beta}\right]\sinh\left[\frac{\pi(x+\imath V_i t)}{V_i\beta}\right]}}\Bigg|_b^c. \tag{51}$$

The appropriate bound b,c is chosen for the Knight shift or for the relaxation rate, and it depends on whether one integrates over a time or a space-time domain.

The results for the Knight shifts, calculated for different atoms and different dopings, are shown in Figs. 10 and 11. The discussion of the relaxation rates is postponed until after the evaluation of the staggered part because the quantity which is measured in experiments is the sum of the uniform and the staggered parts of the relaxation rate.

For the $C1S0$ phase, an activated behavior $\exp(-\frac{\Delta}{T})$ is seen for the Knight shifts of all the atoms. This is shown clearly in the logarithmic plots in the inset of Fig. 10. However let us stress that in the $C1S0$ case we have two spin gaps, so one expects a more complicated shape than a simple straight line. For higher temperatures the Knight shift saturates to a constant value. As expected for the uniform susceptibility, the responses of the different atoms are similar; only their amplitudes are different (this is because of the $|\widetilde{\lambda_{m\nu}}|^2$ coefficients). For larger dopings there are less electrons in the conduction band and their velocity is smaller, so the saturation value also decreases. As the doping increases, spin gaps decrease and curves saturate at a lower T until we reach the quantum critical point (QCP) at $\delta = \delta_{c1}$. This behavior for the susceptibility is described in Ref. 23. In that case, a QCP appears in the presence of $V_{\text{Cu-Cu}}$; in our case, doping drives the transition.

For the $C2S1$ phase, we obtain a finite susceptibility even at zero temperature. This feature comes from the massless spin mode. The central oxygen atom which is coupled only to the gapped band does not give a finite susceptibility at $T=0$. For the second, massive mode we observe a behavior similar to the one described above for the $C1S0$ phase, with the single activation gap shown on the inset of Fig. 10(b) for two dopings.

For the intermediate doping $C2S2$ phase, including logarithmic corrections is the only way to generate some weak T

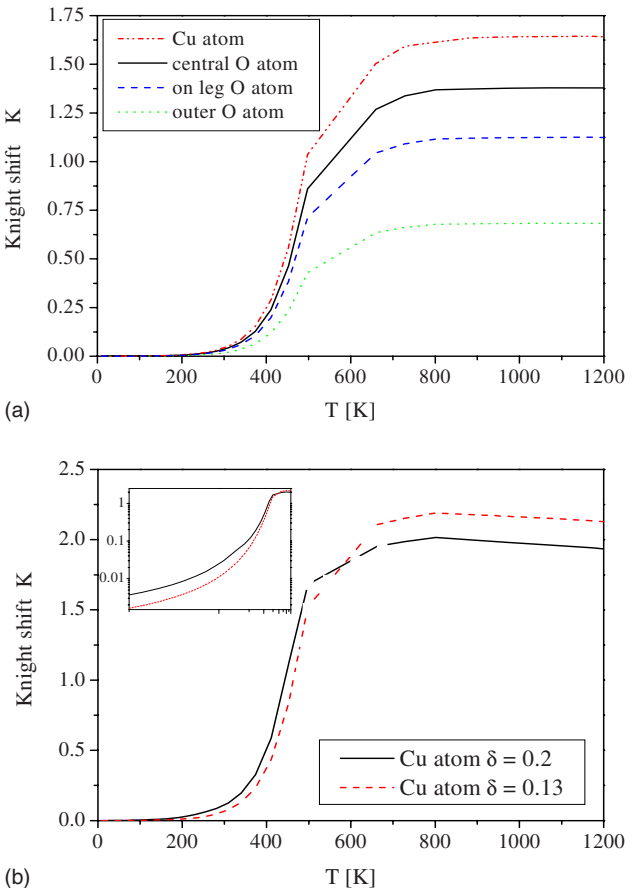

FIG. 10. (Color online) Temperature dependence of the Knight shifts for (a) the different atoms in the elementary cell and (b) different dopings in the $C1S0$ phase. The activation gap at low T is shown in the inset.

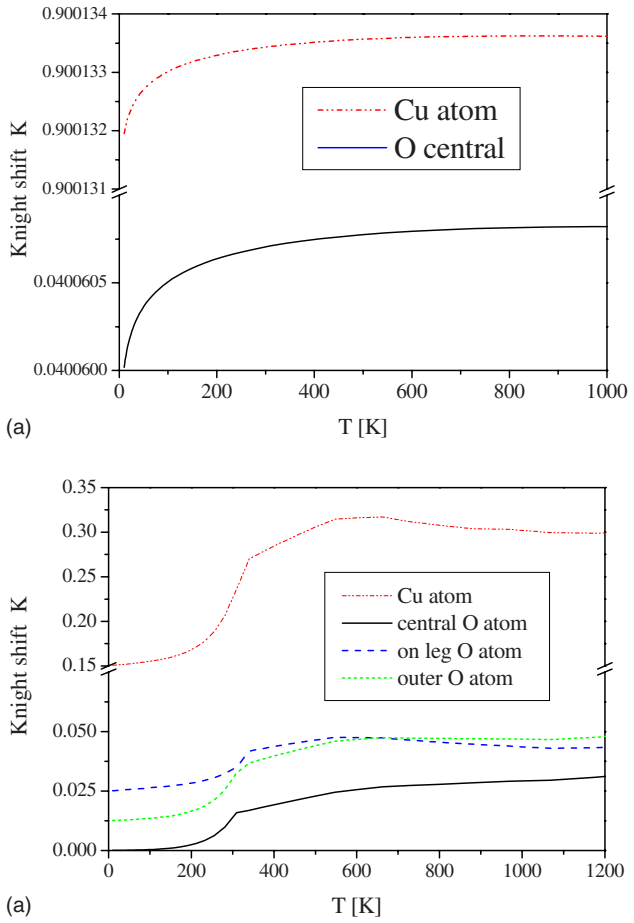

FIG. 11. (Color online) Temperature dependence of the Knight shifts for the different atoms in the elementary cell (a) in the $C2S2$ phase and (b) in the $C2S1$ phase.

dependence. They arise mainly from the presence of the marginal g_1 and g_2 terms. Their influence on the uniform susceptibility is described in detail in Refs. 23 and 88. Differences in the amplitudes of the Knight shifts for the various atoms in the elementary cell stay pretty much the same from one phase to the next, since these amplitudes are simply determined by $\tilde{\lambda}$ coefficients.

2. Staggered part

For $q=2k_F$, both the spin and charge parts contribute to the band-correlation functions. The band $\tilde{R}_{o/\pi}$ with $2k_F$ wave vector is a product of a spin and a charge part, $R_\alpha = R^\sigma_\alpha R^\rho_\alpha$. The form of $F[\phi_\nu]$ depends on the fixed-point eigenbasis for the angles and on the possible existence of gaps.

The expression for the gapped spin phase was obtained using the expression for the $2k_F$ part of the spin-density operator correlations, which is given by $\langle O_{o/\pi \mathrm{SDW}}(r) O_{o/\pi \mathrm{SDW}}(0)\rangle^{2k_F} \sim \cos(\phi_1 \pm \phi_2)$. The last form could be evaluated using the fact that $\phi_i = \phi_{oi} + \delta\phi_i$, where the fluctuations of $\delta\phi_i$ are described by a massive Gaussian model, as was shown in the case of the uniform part. For gapped spin (σ) modes, there are two possibilities:

$$\tilde{R}^\sigma_{o/\pi} = \sinh[K_2\kappa_0(m_2 r_2) \pm K_1\kappa_0(m_1 r_1)] \times (m_2 a)^{K_2}(m_1 a)^{K_1} \quad \text{for the } C1S0 \text{ phase},$$

$$\tilde{R}^\sigma_o = \sinh[K_2\kappa_0(m_2 r_2)](m_2 a)^{K_2} \quad \text{for the } C2S1 \text{ phase}. \tag{52}$$

In the gapless case, one gets a power-law behavior. For the high-T limit of the $C1S0$ phase, where the B_{+-} eigenbasis is relevant, we find

$$\tilde{R}_\alpha = \left(\frac{1}{r_i}\right)^{K_i/2}\left(\frac{1}{r_j}\right)^{K_j/2}, \tag{53}$$

where α corresponds to the band index and $i=1,3$ and $j=2,4$ are the LL modes.

For the $C1S0$ phase, the charge mode is only partially gapped: The field θ_3 is locked so the charge-antisymmetric mode does not give any contribution to SDW, but the massless, "4" (charge-symmetric) mode gives a power-law contribution

$$\tilde{R}^\rho_{o/\pi} = \left(\frac{1}{r}\right)^{K_4/2}. \tag{54}$$

For the other phases, both charge modes are massless. In this case, $B_{o\pi}$ is the fixed-point basis, and we have

$$\tilde{R}_o = \left(\frac{1}{r_j}\right)^{K_4}, \tag{55}$$

$$\tilde{R}_\pi = \left(\frac{1}{r_i}\right)^{K_3}. \tag{56}$$

For the spin part in the $C2S1$ phase, one substitutes K_1, K_2 for K_3, K_4. The amplitudes of $\tilde{R}_\alpha$ on different atoms need to be calculated. Once again $\tilde{\lambda}_{m\alpha}(k)$ are involved. However for those atoms with neighbors along the ladder (on-leg Cu and O atoms), these coefficients are different because of phase factors at $k=2k_F$, which cause cancellations in some contributions of neighboring atoms. Another possible factor may cause differences between atoms in the elementary cell. Following Ref. 89, one may assume that below a characteristic distance $x < L_\delta = \delta^{-1}$, umklapp terms are relevant and that they open up a gap in the charge-symmetric channel. This massive charge correlation affects the staggered part of the magnetic susceptibility, and yields an expression similar to Eq. (52) (with cosh instead of sinh). For on-leg oxygens, which sit between two Cu along the ladder, one recovers a sinh instead of a cosh. This produces different amplitudes $\tilde{R}^\rho_{o/\pi}(L)$ for Cu and for O on-leg atoms provided $L_\delta > m_4^{-1}$. We have made the calculation for the half-filled case, and the result is that m_4 is of the same order as m_2. Thus for dopings larger than 0.05, this effect should not play any role. Once band-correlation functions are known, one may follow exactly the same procedure as in the uniform case in order to obtain the temperature dependence of $\frac{1}{T_1}$.

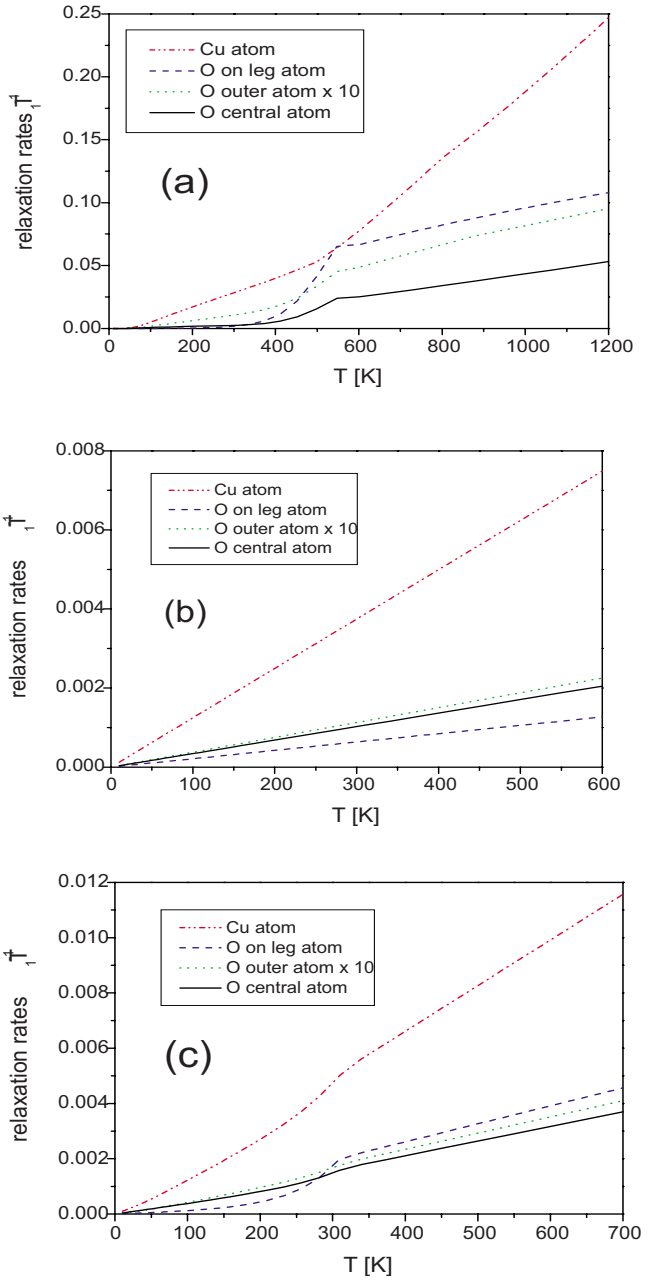

FIG. 12. (Color online) Temperature dependence of the relaxation rates for the different atoms in the elementary cell (a) in the $C1S0$ phase, (b) in the $C2S2$ phase, and (c) in the $C2S1$ phase.

3. Total relaxation rate

The plots in Fig. 12 show $1/T_1$ for different atoms in the elementary cell. They were obtained by numerical integration of Eq. (52) and adding the result to that computed for the uniform part.

As for the Knight shifts, the difference between atoms are caused mainly by the different $\tilde{\lambda}_{m\alpha}$ coefficients. However these coefficients can be different for the staggered part and for the uniform part.

The first observation is the linear dependence of $\frac{1}{T_1}$ at high temperatures for all atoms, for all dopings. The Knight shift saturates in this temperature range to a constant value, and this is in accordance with the Korringa law. For the $C2S2$ phase we observe the linear dependence as expected for a massless LL with all K parameters close to 1.

The second main conclusion is that processes involving large $k_\parallel$ transfers can strongly affect the measured rates, especially for temperatures comparable with the spin gaps, as previously reported.[90] One observes only small differences between atoms in the elementary cell at low T. The difference between the relaxation rate of a Cu nucleus and that of a central O nucleus comes from the fact that the latter may relax only through processes in the "π" band, while for the former, both bands contribute. The difference between on-leg atoms and atoms sitting at other locations comes from the fact that the staggered part contribution of the former nucleus is very small, as it is suppressed by the opposite contributions of the two neighboring Cu atoms. The low-T activation behavior (in the $C2S1$ and $C1S0$ phases) is then clearly seen on these on-leg O sites.

Two points should be kept in mind when comparing our results with experiments. First our Λ_0 is on the order of 0.5 eV, so that the largest charge-antisymmetric gap is on the order of 700 K. Observing it would be experimentally challenging, and it would be even harder to reach the Korringa regime predicted at higher T. Second, our calculations were made in the phase where SCd fluctuations dominate. Thus experiments done at large pressures would be the most relevant to compare our findings with. Aside from the above caveats, the results of our calculations seem to be in very reasonable agreement with experiments.[10,11]

VII. CONCLUSIONS

Our study has clearly shown that including oxygen atoms in the structure produces significant changes in the ground-state phase diagram of doped Cu-O two-leg Hubbard ladders. This result is fully consistent with DMRG studies suggesting that there are quantitative differences between models which include O atoms and models which do not, even close to half filling. The massless $C2S2$ phase is of special importance in that respect. A *Varma-type* phase with incommensurate orbital current patterns and an additional density wave characterize the ground-state structure at intermediate and large dopings. The signatures of these states can be seen in NMR experiments probing the various nuclei in the cell.

We see important differences between Cu and Cu-O ladders in the weak-interaction limit ($U < \epsilon$). However numerical approaches which can investigate the opposite limit as well suggest that these differences do survive for $U > \epsilon$. This invites further analytical studies of the two-leg Cu-O Hubbard ladders in the large U limit.

ACKNOWLEDGMENTS

This work was supported in part by the Swiss National Science Foundation under MaNEP and Division II and by an ESRT Marie Curie grant.

APPENDIX A: COUPLING CONSTANTS

The initial conditions for the nonlinear terms are

$$g_{1c}^{o} = 4f(1,2,1,2,1),$$

$$g_{1a}^{o} = 4f(1,2,2,1,1),$$

$$g_{2c}^{o} = 4f(1,2,1,2,-1),$$

$$g_{\|c}^{o} = 4[f(1,2,1,2,1) - f(1,2,1,2,-1)],$$

$$g_{1}^{o} = \frac{2f(1,1,1,1,1)}{V_{Fo}} + \frac{2f(2,2,2,2,1)}{V_{F\pi}},$$

$$g_{2}^{o} = \frac{2f(1,1,1,1,1)}{V_{Fo}} - \frac{2f(2,2,2,2,1)}{V_{F\pi}},$$

$$g_{4a}^{o} = 4f(1,2,2,1,-1), \tag{A1}$$

where the function $f(k,l,m,n,p)$ converts the interactions given in the atomic basis $(U_{\mathrm{Cu}}, U_{\mathrm{O}}, V_{\mathrm{Cu\text{-}O}})$ into band g-ology interactions:

$$f(k,l,m,n,p) = \sum_{i,j} \lambda_{ik}^{*}\lambda_{il}^{*}\lambda_{jm}\lambda_{jn}[V^{\mathrm{intra}} + V^{\mathrm{inter}}\cos(k_{Fm} - pk_{Fn})]. \tag{A2}$$

The summation is taken over all the atoms in the elementary cell. V^{intra} denotes interactions within the elementary cell, and V^{inter} is $V_{\mathrm{Cu\text{-}O}}$, since one of the atoms is outside the elementary cell, as in Ref. 49. Initial values for K and $\cot(\alpha), \cot(\beta)$ are evaluated as follows: Starting from Eq. (12), one performs a $S(\pi/4)$ rotation. In this B_{+-} basis, $\hat{K}$ can be calculated by simply solving a matrix equation. The initial K_{ν} are given by the eigenvalues of this matrix, and $\cot(\alpha), \cot(\beta)$ are the ratios of nondiagonal terms to the difference of diagonal ones. For example, $\cot(\alpha) = 2B_{s+,s-}/(K_{s-} - K_{s+})$.

The system of RG differential equations is solved by means of an iterative method. If $\cot(\alpha)$ [or $\cot(\beta)$] becomes very large during the flow, we stop the flow at some point, introduce the tangent of the angles instead of the cotangent, and then resume the iteration scheme. In this way, we are able to isolate divergences of the prefactors in some of the cosine terms, which cause gaps to open and affect observables.

APPENDIX B: DERIVATION OF THE RG EQUATIONS

1. Flow of the diagonal basis

To second order in perturbation, one finds the corrections dK_1, dK_2, dK_3, and dK_4 to the LL parameters and the nondiagonal terms dB_{12} and dB_{34}. These nondiagonal terms signal that after the RG step, B_o is no longer a diagonal basis. We then go back to the B_{+-} basis, using the transformation S^{-1}. In this basis, off-diagonal terms have been incremented by small amounts during the RG step. For instance,

$$dB_{s-s+} = -\frac{1}{2}(dK_1 - dK_2)\cos 2\alpha + dB_{12}\sin 2\alpha. \tag{B1}$$

Diagonal terms also undergo infinitesimal variations,

$$dK_{s-(s+)} = \frac{1}{2}(dK_1 + dK_2) \pm \frac{1}{2}[2dB_{12}\cos 2\alpha + (dK_1 - dK_2)\sin 2\alpha]. \tag{B2}$$

Similar expressions hold for the charge modes when we perform the substitutions $s \to c$, $1 \to 3$, $2 \to 4$, and $\alpha \to \beta$ in the equations above.

The new matrix is diagonalized by the operator $S(\alpha + d\alpha, \beta + d\beta)$, where the angle $d\alpha$, which accounts for the $dB_{\mu-\mu+}$ and $dK_{\mu-(\mu+)}$ variations $(\mu = c,s)$, indicate a rotation of B_o. This idea is summarized in the diagram shown in Fig. 3.

We now determine the renormalization flow of the angles α and β. In the spin sector, the diagonalization condition is written in terms of $K_{s-(s+)}$ and B_{s-s+},

$$\frac{1}{2}(K_{s-} - K_{s+})\cos 2\alpha + B_{s-s+}\sin 2\alpha = 0. \tag{B3}$$

One differentiates the above equation in order to relate $d\alpha$, $K_{s-(s+)}$, and B_{s-s+}:

$$-\frac{d2\alpha}{\sin^2 2\alpha} = \frac{2}{K_{s-} - K_{s+}} \frac{\frac{1}{2}(dK_{s-} - dK_{s+})\cos 2\alpha - dB_{s-s+}\sin 2\alpha}{(\sin^2 2\alpha - \cos^2 2\alpha)\sin 2\alpha}. \tag{B4}$$

In the diagonal basis this equation reads

$$d\cot 2\alpha = -\frac{1}{K_1 - K_2}\left[(dK_1 - dK_2)\frac{2\sin 2\alpha \cos 2\alpha}{\sin^2 2\alpha - \cos^2 2\alpha} - dB_{12}\frac{-\sin^2 2\alpha + \cos^2 2\alpha}{\sin^2 2\alpha - \cos^2 2\alpha}\right], \tag{B5}$$

where the differentials of the LL parameters are known in the diagonal basis. They were obtained to second order in perturbation, and the dK_{ν}, which we use here, were given in Sec. III A. In the charge sector, we obtain the equivalent set of equations with the changes $s \to c$, $1 \to 3$, $2 \to 4$, and $\alpha \to \beta$. The additional expressions for the differentials of off-diagonal terms are obtained in a similar way, giving for the case of a generic filling,

$$dB_{12} = P_1Q_1[(g_{1a}^2 + g_{\|c}^2 + G_t^2) - K_1K_2(g_{1a}^2 + g_{1c}^2 + g_{2c}^2 + G_p^2)] - K_1K_2h(P_1)g_1g_2,$$

$$dB_{34} = P_2Q_2(g_{1c}^2 + g_{2c}^2 + g_{\|c}^2), \tag{B6}$$

where $h(P_1) = [(P_1Q_1)^2 + 0.25(P_1^2 - Q_1^2)]^{-1}$.

2. First-order correction to g_1 and g_2

Setting $g_1=g_{1d}+g_{1d'}$ and $g_2=g_{1d}-g_{1d'}$, the Hamiltonian reads

$$H = H_{\mathrm{LL}} + g_1 \int dr \cos(2\phi_{s-})\cos(2\phi_{s+}) + g_2 \int dr \sin(2\phi_{s-})\sin(2\phi_{s+}). \tag{B7}$$

In order to simplify the RG calculation, we first solve this problem in the total/transverse basis, where the averages over the high-energy terms are $\langle \phi_{s-}(r)^2\rangle_h = K_{s-}dl$, $\langle \phi_{s+}(r)^2\rangle_h = K_{s+}dl$, and $\langle \phi_{s-}(r)\phi_{s+}(r)\rangle_h = \frac{1}{2}Adl$. One may determine the renormalization flow that is produced when integrating out the high-energy components. For instance, the renormalization of g_1 gives

$$\langle g_1 \int dr \cos[2(\phi_{s+}+h[\phi_{s+}])]\cos[2(\phi_{s-}+h[\phi_{s-}])]\rangle_h = \frac{1}{2}g_1\langle \int dr \cos[2(\phi_{s+}+\phi_{s-})+(h[\phi_{s+}]+h[\phi_{s-}])]\rangle_h + \langle \int dr \cos[2(\phi_{s+}-\phi_{s-})+(h[\phi_{s+}]-h[\phi_{s-}])]\rangle_h. \tag{B8}$$

We re-exponentiate the cosines, use Debye-Waller-type relations, and expand the exponential function in the Taylor series,

$$\begin{aligned}\langle \cos(x+h[x])\rangle_h &= \cos(x)\langle \sum_{\sigma=\pm} \exp(2\imath\sigma h[x])\rangle_h \\ &= \cos(x)\exp(-\langle h[x]^2\rangle_h) \\ &= (1-\langle h[x]^2\rangle_h)\cos(x),\end{aligned} \tag{B9}$$

where $\langle (h[\phi_{s+}]\pm h[\phi_{s-}])^2\rangle_h = (K_{s+}+K_{s-})dl \pm Adl$. One then finds the usual diagonal term

$$\begin{aligned}g_1[1-(K_{s+}+K_{s-})dl]\int dr\{&\cos[2(\phi_{s+}+\phi_{s-})] \\ &+\cos[2(\phi_{s+}-\phi_{s-})]\} \\ &= 2g_1[1-(K_{s+}+K_{s-})dl]\int dr \cos(2\phi_{s+})\cos(2\phi_{s-}).\end{aligned} \tag{B10}$$

After rescaling the integration variable dr, one gets the RG equation for g_1. However in the nondiagonal basis there is also an additional term,

$$\begin{aligned}g_1 A dl \int dr[\cos(2(\phi_{s+}+\phi_{s-}))-\cos(2(\phi_{s+}-\phi_{s-}))] \\ = -2g_1 A dl \int dr \sin(2\phi_{s-})\sin(2\phi_{s+}).\end{aligned} \tag{B11}$$

This links the change in g_2 to the coupling constant g_1. The derivation of the RG equation for the g_2 term is obtained in a similar fashion, using the identity

$$\sin(2\phi_{s+})\sin(2\phi_{s-}) = \frac{1}{2}[\cos(\phi_{s+}-\phi_{s-})-\cos(\phi_{s+}+\phi_{s-})]. \tag{B12}$$

Finally, the first-order RG equation for g_1 is

$$\frac{dg_{1(2)}}{dl} = g_{1(2)}[2-(K_{s+}+K_{s-})]+g_{2(1)}A. \tag{B13}$$

In the diagonal basis, using

$$\begin{aligned}K_{s-(2)} &\to P^2K_{1(2)}+2PQA_{12}+Q^2K_{2(1)}, \\ A &\to PQ(K_1-K_2)+A_{12}(P^2-Q^2),\end{aligned} \tag{B14}$$

the RG equations for the couplings are

$$\frac{dg_{1(2)}}{dl} = g_{1(2)}(K_2+K_1)+g_{2(1)}[(P^2-Q^2)A_{12}+PQ(K_1-K_2)]. \tag{B15}$$

3. RG equations for the half-filled case

Using the same method as for the incommensurate case, we find the following system of equations:

$$\begin{aligned}\frac{dK_1}{dl} = \frac{1}{2}\Big\{ & P_1^2[g_{1a}^2+J_0(\delta)g_{3a}^2+g_{\|c}^2+G_t^2] \\ & -K_1^2\Big[Q_1^2g_{1a}^2+J_0(\delta)Q_1^2g_{3l}^2+Q_1^2g_{1c}^2+P_1^2G_p^2+P_1^2g_{2c}^2 \\ & +J_0(\delta)P_1^2g_{3b}^2+\frac{1}{2}(g_1^2+g_2^2)+f(P_1)(g_1g_2)\Big]\Big\},\end{aligned}$$

$$\begin{aligned}\frac{dK_2}{dl} = \frac{1}{2}\Big\{ & Q_1^2[g_{1a}^2+J_0(\delta)g_{3a}^2+g_{\|c}^2+G_t^2] \\ & -K_2^2\Big[P_1^2g_{1a}^2+P_1^2g_{1c}^2+J_0(\delta)P_1^2g_{3\|}^2+Q_1^2G_p^2 \\ & +J_0(\delta)Q_1^2g_{3b}^2+Q_1^2g_{2c}^2+\frac{1}{2}(g_1^2+g_2^2)-f(P_1)(g_1g_2)\Big]\Big\},\end{aligned}$$

$$\begin{aligned}\frac{dK_3}{dl} = & \frac{1}{2}P_2^2(g_{1c}^2+g_{2c}^2+g_{\|c}^2+g_{3c}^2)+\frac{1}{2}Q_2^2(g_{3\|}^2+g_{3a}^2+g_{3b}^2 \\ & +g_{3c}^2)J_0(\delta),\end{aligned}$$

$$\begin{aligned}\frac{dK_4}{dl} = & \frac{1}{2}Q_2^2(g_{1c}^2+g_{2c}^2+g_{\|c}^2+g_{3c}^2)+\frac{1}{2}P_2^2(g_{3\|}^2+g_{3a}^2+g_{3b}^2 \\ & +g_{3c}^2)J_0(\delta),\end{aligned}$$

$$\begin{aligned}\frac{dg_{1c}}{dl} = & g_{1c}[2-(P_1^2K_2+P_2^2K_3^{-1}+Q_1^2K_1+Q_2^2K_4^{-1})] \\ & -[g_1g_{2c}+g_{1a}g_{\|c}+J_0(\delta)g_{3c}g_{3\|}],\end{aligned}$$

$$\frac{dg_{1a}}{dl} = g_{1a}\{2 - [P_1^2(K_2 + K_1^{-1}) + Q_1^2(K_1 + K_2^{-1})]\} - [g_{1c}g_{\|c} + J_0(\delta)g_{3a}g_{3\|}],$$

$$\frac{dg_{2c}}{dl} = g_{2c}[2 - P^2(P_2^2K_3^{-1} + P_1^2K_1 + Q_2^2K_4^{-1} + Q_1^2K_2)] - [g_{1c}g_1 + J_0(\delta)g_{3c}g_{3a}],$$

$$\frac{dg_1}{dl} = g_1[2 - (K_2 + K_1)] + P_1Q_1(K_2 - K_1)g_2 - \gamma[g_{1c}g_{2c} + J_0(\delta)g_{3b}g_{3\|}],$$

$$\frac{dg_2}{dl} = g_2[2 - (K_2 + K_1)] + P_1Q_1(K_2 - K_1)g_1,$$

$$\frac{dg_{\|c}}{dl} = g_{\|c}[2 - (P_1^2K_1^{-1} + Q_1^2K_2^{-1} + P_2^2K_3^{-1} + Q_2^2K_4^{-1})] - [g_{1a}g_{1c} + J_0(\delta)g_{3a}g_{3c}],$$

$$\frac{dg_{4a}}{dl} = g_{4a}\left\{2 - \frac{1}{2}[P_1^2(K_1 + K_1^{-1}) + Q_1^2(K_2 + K_2^{-1})]\right\},$$

$$\frac{dG_p}{dl} = G_p[1 - (P_1^2K_1 + Q_1^2K_2)] + g_{4a}^2[P_1^2(K_1 - K_1^{-1}) + Q_1^2(K_2 - K_2^{-1})],$$

$$\frac{dG_t}{dl} = G_t[1 - (P_1^2K_1^{-1} + Q_1^2K_2^{-1})] + g_{4a}^2[P_1^2(-K_1 + K_1^{-1}) + Q_1^2(-K_2 + K_2^{-1})],$$

$$\frac{dg_{3\|}}{dl} = g_{3\|}[2 - (P_1^2K_2 + P_2^2K_4 + Q_1^2K_1 + Q_2^2K_3)] - (g_1g_{3b} + g_{1c}g_{3c} + g_{1a}g_{3a}),$$

$$\frac{dg_{3a}}{dl} = g_{3a}[2 - (P_1^2K_1^{-1} + P_2^2K_4 + Q_1^2K_2^{-1} + Q_2^2K_3)] - (g_{\|c}g_{3c} + g_{1a}g_{3\|}),$$

$$\frac{dg_{3b}}{dl} = g_{3b}[2 - (P_1^2K_1 + P_2^2K_4 + Q_1^2K_2 + Q_2^2K_3)] - (g_1g_{3\|} + g_{2c}g_{3c}),$$

$$\frac{dg_{3c}}{dl} = g_{3c}\{2 - [P_2^2(K_4 + K_3^{-1}) + Q_2^2(K_3 + K_4^{-1})]\} - (g_{\|c}g_{3a} + g_{2c}g_{3b} + g_{1c}g_{3\|}), \tag{B16}$$

where

$$f(P_1) = \left(P_1Q_1 + \frac{1}{4}\frac{P_1^2 - Q_1^2}{P_1Q_1}\right)^{-1}. \tag{B17}$$

The renormalization of the parameter γ is controlled by the same equation as before. The additional flows for the velocities of the modes, due to umklapp scattering, are all proportional to a Bessel term $J_2(4\delta)$ and hence are neglected. The general formula describing the flow of the diagonal basis remains the same as for the incommensurate case. However one needs to substitute modified expressions of the dK_ν.

APPENDIX C: ORDER PARAMETER OPERATORS IN BOSONIZATION LANGUAGE

We first write the order parameters in fermionic language. We consider only those order parameters which can produce power-law decays of correlations for the various locked phase fields combinations. These operators are first defined for each site then expressed in the o/π basis, where the $\lambda_{m\alpha}$ coefficients enter their expressions.

There are two kinds of order parameter operators. The first group represents charge-density (particle-hole) fluctuations with a $2k_F$ wave vector. They correspond to the usual CDW, which is the sum of CDW in each band. Up to an unimportant constant factor it gives

$$O_{\mathrm{CDW}} \sim \sum_{\mu}\sum_{\sigma\sigma'} \alpha^{\dagger}_{-\mu\sigma}\delta_{\sigma\sigma'}\alpha_{+\mu\sigma'}. \tag{C1}$$

The subscript μ denotes the band, so to obtain the order parameter inside one specific band, it is enough to take the first or the second term in the above sum. It is also possible to define an operator which describes the difference of the densities on the two legs,

$$O_{\pi\mathrm{CDW}} \sim \sum_{\mu}\sum_{\sigma\sigma'} \alpha^{\dagger}_{-\bar{\mu}\sigma}\delta_{\sigma\sigma'}\alpha_{+\mu\sigma'}, \tag{C2}$$

or the operator which describes an orbital antiferromagnetic (OAF) fluctuation where currents flow along the legs and the rungs of the ladder,

$$O_{\mathrm{OAF}} \sim \sum_{\mu}\sum_{\sigma\sigma'} \mu\alpha^{\dagger}_{-\bar{\mu}\sigma}\delta_{\sigma\sigma'}\alpha_{+\mu\sigma'}, \tag{C3}$$

We can also define (at half filling) "bond" operators, which represent density waves located on the bonds, either in phase,

$$O_{\mathrm{BDW}} \sim \sum_{\mu}\sum_{\sigma\sigma'} \exp(ik_{F\mu}x)\alpha^{\dagger}_{-\mu\sigma}\delta_{\sigma\sigma'}\alpha_{+\mu\sigma'}, \tag{C4}$$

out of phase between the two legs of the ladder,

$$O_{\pi\mathrm{BDW}} \sim \sum_{\mu}\sum_{\sigma\sigma'} \exp(ik_{F\mu}x)\alpha^{\dagger}_{-\bar{\mu}\sigma}\delta_{\sigma\sigma'}\alpha_{+\mu\sigma'}, \tag{C5}$$

or in the diagonal direction,

$$O_{\mathrm{FDW}} \sim \sum_{\mu}\sum_{\sigma\sigma'} \exp(ik_{F\mu}x)\mu\alpha^{\dagger}_{-\bar{\mu}\sigma}\delta_{\sigma\sigma'}\alpha_{+\mu\sigma'}. \tag{C6}$$

Away from half filling, on-site and bond operators are degenerate because of translational invariance (the charge-symmetric mode is massless).

The second group describes superconducting pairing (particle-particle) fluctuations with zero wave vectors. As usual there is the s-wave pairing

$$O_{\mathrm{SCs}} \sim \sum_{\mu} \sum_{\sigma\sigma'} \sigma \alpha_{-\bar{\mu}\bar{\sigma}} \delta_{\sigma\sigma'} \alpha_{+\mu\sigma'}, \tag{C7}$$

and the d-wave pairing, which corresponds to a change of the sign of the order parameter when moving from along the legs to along the rungs,

$$O_{\mathrm{SCd}} \sim \sum_{\mu} \sum_{\sigma\sigma'} \sigma\mu \alpha_{-\mu\bar{\sigma}} \delta_{\sigma\sigma'} \alpha_{+\mu\sigma'}. \tag{C8}$$

These phases are given different names in the literature. The name *orbital antiferromagnet* was used traditionally for the operator defined above, but it is also called staggered flux[24] (SF) or d-density-wave[68] (DDW) phase. Its bond counterpart is sometimes called f-density-wave[24] (FDW) or diagonal current[68] (DC) phase. Similarly, our πCDW and πBDW orders are also denoted[24] CDW and π-density wave (PDW) or CDW and SP in Ref. 68. We have decided to use the notation πCDW to avoid any confusion with the usual CDW, which also appears in our calculation.

We can now represent the operators in terms of boson fields, using mapping equation (8). It is important to keep the same convention for the signs of the Klein factors as that we used to write the Hamiltonian in bosonic form. Choosing $\Gamma = +1$, we get $\eta_{\sigma+}\eta_{\sigma-} = +\imath$. This determines whether a sine or a cosine appears in the formulas below. This choice was used in Refs. 24 and 49 but the opposite one was used in Ref. 89. One can easily relate the two by shifting the phase fields ϕ by an amount $\pi/2$.

The operators take the form

$$\begin{aligned}
O_{\pi\mathrm{CDW}} &\sim \cos\phi_{c+} \sin\theta_{c-} \cos\phi_{s+} \cos\theta_{s-} \\
&\quad - \sin\phi_{c+} \cos\theta_{c-} \sin\phi_{s+} \sin\theta_{s-}, \\
O_{\mathrm{OAF}} &\sim \cos\phi_{c+} \cos\theta_{c-} \cos\phi_{s+} \cos\theta_{s-} \\
&\quad + \sin\phi_{c+} \sin\theta_{c-} \sin\phi_{s+} \sin\theta_{s-}, \\
O_{\pi\mathrm{BDW}} &\sim \cos\phi_{c+} \cos\theta_{c-} \sin\phi_{s+} \sin\theta_{s-} \\
&\quad + \sin\phi_{c+} \sin\theta_{c-} \cos\phi_{s+} \cos\theta_{s-}, \\
O_{\mathrm{FDW}} &\sim \cos\phi_{c+} \sin\theta_{c-} \sin\phi_{s+} \sin\theta_{s-} \\
&\quad - \sin\phi_{c+} \cos\theta_{c-} \cos\phi_{s+} \cos\theta_{s-}, \\
O_{\mathrm{SCs}} &\sim \exp\imath\theta_{c+} \cos\theta_{c-} \sin\phi_{s+} \sin\phi_{s-} \\
&\quad - \imath \exp\imath\theta_{c+} \sin\theta_{c-} \cos\phi_{s+} \cos\phi_{s-}, \\
O_{\mathrm{SCd}} &\sim \exp\imath\theta_{c+} \cos\theta_{c-} \cos\phi_{s+} \cos\phi_{s-} \\
&\quad - \imath \exp\imath\theta_{c+} \sin\theta_{c-} \sin\phi_{s+} \sin\phi_{s-}.
\end{aligned} \tag{C9}$$

It is also useful to consider these operators in the $B_{o\pi}$ basis. For example, the SDW operator in the o-band SDW(o) and the CDW operator in the π-band CDW(π) are

$$\begin{aligned}
O_{\mathrm{SDW}(o)} &\sim \exp\imath(\phi_{c+} + \phi_{c-}) \sin(\phi_{s+} + \phi_{s-}), \\
O_{\mathrm{CDW}(\pi)} &\sim \exp\imath(\phi_{c+} - \phi_{c-}) \cos(\phi_{s+} - \phi_{s-}).
\end{aligned} \tag{C10}$$

To determine the phases, we need to obtain the exponents that characterize the spatial decay of the operators' correlations. Using a standard procedure to compute the correlations with the quadratic Hamiltonian,[8] we find

$$\begin{aligned}
\eta_{\mathrm{CDW}} &= K_2 + K_1 + K_4 + K_3, \\
\eta_{\mathrm{OAF}} &= P_1^{*2} K_2 + Q_1^{*2} K_1 + P_1^{*2} K_1^{-1} + Q_1^{*2} K_2^{-1} + P_2^{*2} K_4 + Q_2^{*2} K_3 \\
&\quad + P_2^{*2} K_3^{-1} + Q_2^{*2} K_4^{-1}, \\
\eta_{\mathrm{SCd}} &= K_2 + K_1 + K_4^{-1} + K_3^{-1}.
\end{aligned} \tag{C11}$$

The exponents of the OAF and πCDW fluctuations are the same, so we need to evaluate logarithmic corrections to the power-law decay to determine the dominant ordering.

APPENDIX D: SIMPLIFIED SYSTEM OF RG EQUATIONS

When $\cot 2\alpha \to 0$ and $\cot 2\beta \to \infty$, one gets the following system of first-order RG equations for the couplings:

$$\begin{aligned}
\frac{dg_{1c}}{dl} &= g_{1c}\left[2 - \left(K_2 + \frac{1}{2}K_3^{-1} + \frac{1}{2}K_4^{-1}\right)\right], \\
\frac{dg_{1a}}{dl} &= g_{1a}[2 - (K_2 + K_1^{-1})], \\
\frac{dg_{2c}}{dl} &= g_{2c}\left[2 - \left(\frac{1}{2}K_3^{-1} + K_1 + \frac{1}{2}K_4^{-1}\right)\right], \\
\frac{dg_1}{dl} &= g_1[2 - (K_2 + K_1)], \\
\frac{dg_2}{dl} &= g_2[2 - (K_2 + K_1)], \\
\frac{dg_{\|c}}{dl} &= g_{\|c}\left[2 - \left(K_1^{-1} + \frac{1}{2}K_3^{-1} + \frac{1}{2}K_4^{-1}\right)\right].
\end{aligned} \tag{D1}$$

The zeroth-order approximation to the above system is obtained using the fact that K_4 (K_2) is much smaller (larger) than one.

For the $C2S1$ phase, the relevance of the important coupling needs to be checked. This gives us only one differential equation in this case (assuming that close to the fixed point, $|g_1| = |g_2| = g$),

$$\frac{dg}{dl} = g[2 - (K_2 + K_1)] + P_1 Q_1 (K_2 - K_1) g. \tag{D2}$$

Taking into account the fact that $P_1 Q_1 < 0$, that it keeps decreasing during the flow, and that the initial K_2 makes g irrelevant, one finds that a significant decrease in K_2 would be required in order to make g relevant.

[1] P. Lee, N. Nagaosa, and X. Wen, Rev. Mod. Phys. **78**, 17 (2006).
[2] S. Hébert, S. Lambert, D. Pelloquin, and A. Maignan, Phys. Rev. B **64**, 172101 (2001).
[3] M. B. Salamon and M. Jaime, Rev. Mod. Phys. **73**, 583 (2001).
[4] G. R. Stewart, Rev. Mod. Phys. **56**, 755 (1984).
[5] E. Dagotto and T. M. Rice, Science **271**, 618 (1996), and references therein.
[6] T. Nagata, M. Uehara, J. Goto, M. Komiya, J. Akimitsu, N. Motoyama, H. Eisaki, S. Uchida, B. Takahasi, T. Nakanishi, and N. Môri, Physica C **282**, 153 (1997).
[7] U. Ledermann, K. Le Hur, and T. M. Rice, Phys. Rev. B **62**, 16383 (2000).
[8] T. Giamarchi, *Quantum Physics in One Dimension* (Oxford University Press, Oxford, 2004).
[9] Y. Piskunov, D. Jérome, P. Auban-Senzier, P. Wzietek, U. Ammerahl, G. Dhalenne, and A. Revcolevschi, Eur. Phys. J. B **13**, 417 (2000).
[10] Y. Piskunov, D. Jérome, P. Auban-Senzier, P. Wzietek, and Y. Yakubovsky, Phys. Rev. B **69**, 014510 (2004).
[11] N. Fujiwara, N. Mōri, Y. Uwatoko, T. Matsumoto, N. Motoyama, and S. Uchida, Phys. Rev. Lett. **90**, 137001 (2003).
[12] T. Imai, K. R. Thurber, K. M. Shen, A. W. Hunt, and F. C. Chou, Phys. Rev. Lett. **81**, 220 (1998).
[13] K. I. Kumagai, S. Tsuji, M. Kato, and Y. Koike, Phys. Rev. Lett. **78**, 1992 (1997).
[14] J. Sólyom, Adv. Phys. **28**, 201 (1979).
[15] C. M. Varma and A. Zawadowski, Phys. Rev. B **32**, 7399 (1985).
[16] K. Penc and J. Sólyom, Phys. Rev. B **41**, 704 (1990).
[17] M. Fabrizio, Phys. Rev. B **48**, 15838 (1993).
[18] K. Kuroki and H. Aoki, Phys. Rev. Lett. **72**, 2947 (1994).
[19] H. J. Schulz, in *Correlated Fermions and Transport in Mesoscopic Systems*, edited by T. Martin, G. Montambaux, and J. Tran Thanh Van (Editions frontières, Gif sur Yvette, France, 1996), p. 81.
[20] L. Balents and M. P. A. Fisher, Phys. Rev. B **53**, 12133 (1996).
[21] H. H. Lin, L. Balents, and M. P. A. Fisher, Phys. Rev. B **56**, 6569 (1997).
[22] U. Ledermann and K. Le Hur, Phys. Rev. B **61**, 2497 (2000).
[23] M. Tsuchiizu and Y. Suzumura, Phys. Rev. B **72**, 075121 (2005).
[24] M. Tsuchiizu and A. Furusaki, Phys. Rev. B **66**, 245106 (2002).
[25] D. Poilblanc, D. J. Scalapino, and W. Hanke, Phys. Rev. B **52**, 6796 (1995).
[26] R. M. Noack, S. R. White, and D. J. Scalapino, Phys. Rev. Lett. **73**, 882 (1994).
[27] B. Srinivasan and M.-B. Lepetit, Phys. Rev. B **66**, 024421 (2002).
[28] N. Nagaosa, Solid State Commun. **94**, 495 (1995).
[29] D. J. Scalapino, S. R. White, and I. Affleck, Phys. Rev. B **64**, 100506(R) (2001).
[30] G. Roux, E. Orignac, S. R. White, and D. Poilblanc, Phys. Rev. B **76**, 195105 (2007).
[31] D. V. Khveshchenko and T. M. Rice, Phys. Rev. B **50**, 252 (1994).
[32] M. Tsuchiizu and Y. Suzumura, Phys. Rev. B **59**, 12326 (1999).
[33] M. Tsuchiizu, P. Donohue, Y. Suzumura, and T. Giamarchi, Eur. Phys. J. B **19**, 185 (2001).
[34] H. Yoshioka and Y. Suzumura, Phys. Rev. B **54**, 9328 (1996).
[35] F. C. Zhang and T. M. Rice, Phys. Rev. B **37**, 3759 (1988).
[36] H. Alloul, J. Bobroff, M. Gabay, and P. Hirschfeld, arXiv:0711.0877, Rev. Mod. Phys. (to be published).
[37] C. M. Varma, Phys. Rev. B **55**, 14554 (1997).
[38] C. M. Varma, Phys. Rev. B **73**, 155113 (2006).
[39] I. Affleck and J. B. Marston, Phys. Rev. B **37**, 3774 (1988).
[40] G. Kotliar and J. Liu, Phys. Rev. B **38**, 5142(R) (1988).
[41] P. Lederer, D. Poilblanc, and T. M. Rice, Phys. Rev. Lett. **63**, 1519 (1989).
[42] F. C. Zhang, Phys. Rev. Lett. **64**, 974 (1990).
[43] E. Orignac and T. Giamarchi, Phys. Rev. B **56**, 7167 (1997).
[44] U. Schollwock, S. Chakravarty, J. O. Fjaerestad, J. B. Marston, and M. Troyer, Phys. Rev. Lett. **90**, 186401 (2003).
[45] A. Nersesyan, A. Luther, and F. Kusmartsev, Phys. Lett. A **176**, 363 (1993).
[46] S. Chakravarty, R. B. Laughlin, D. K. Morr, and C. Nayak, Phys. Rev. B **63**, 094503 (2001).
[47] B. Fauqué, Y. Sidis, V. Hinkov, S. Pailhès, C. T. Lin, X. Chaud, and P. Bourges, Phys. Rev. Lett. **96**, 197001 (2006).
[48] J. Xia, E. Schemm, G. Deutscher, S. A. Kivelson, D. A. Bonn, W. N. Hardy, R. Liang, W. Siemons, G. Koster, M. M. Fejer, and A. Kapitulnik, Phys. Rev. Lett. **100**, 127002 (2008).
[49] S. Lee, J. B. Marston, and J. O. Fjaerestad, Phys. Rev. B **72**, 075126 (2005).
[50] E. Jeckelmann, D. J. Scalapino, and S. R. White, Phys. Rev. B **58**, 9492 (1998).
[51] P. Chudzinski, M. Gabay, and T. Giamarchi, Phys. Rev. B **76**, 161101(R) (2007).
[52] T. F. A. Müller, V. Anisimov, T. M. Rice, I. Dasgupta, and T. Saha-Dasgupta, Phys. Rev. B **57**, R12655 (1998).
[53] J. Voit, Rep. Prog. Phys. **57**, 977 (1995).
[54] Y. Fuseya, M. Tsuchiizu, Y. Suzumura, and C. Bourbonnais, J. Phys. Soc. Jpn. **76**, 014709 (2007).
[55] H. Nélisse, C. Bourbonnais, H. Touchette, Y. Vilk, and A.-M. Tremblay, Eur. Phys. J. B **12**, 351 (1999).
[56] T. Giamarchi, Phys. Rev. B **44**, 2905 (1991).
[57] T. Giamarchi, Physica B **230-232**, 975 (1997), and references therein.
[58] S. Wessel, M. Indergand, A. Lauchli, U. Ledermann, and M. Sigrist, Phys. Rev. B **67**, 184517 (2003).
[59] R. Rajaraman, *Solitons and Instantons: An Introduction to Solitons and Instantons in Quantum Field Theory* (North-Holland, Amsterdam, 1982).
[60] K. Penc and F. Mila, Phys. Rev. B **50**, 11429 (1994).
[61] H. H. Lin, L. Balents, and M. P. A. Fisher, Phys. Rev. B **58**, 1794 (1998).
[62] D. Controzzi and A. M. Tsvelik, Phys. Rev. B **72**, 035110 (2005).
[63] D. G. Shelton and D. Senechal, Phys. Rev. B **58**, 6818 (1998).
[64] S. Nishimoto and Y. Ohta, Phys. Rev. B **68**, 235114 (2003).
[65] S. Baruch and D. Orgad, Phys. Rev. B **71**, 184503 (2005).
[66] T. Fukui, M. Sigrist, and N. Kawakami, Phys. Rev. B **56**, 2530 (1997).
[67] J. Voit, Phys. Rev. B **45**, 4027 (1992).
[68] C. Wu, W. V. Liu, and E. Fradkin, Phys. Rev. B **68**, 115104 (2003).
[69] V. J. Emery, S. A. Kivelson, and O. Zachar, Phys. Rev. B **59**, 15641 (1999).
[70] Y. Park, S. Liang, and T. K. Lee, Phys. Rev. B **59**, 2587 (1999).
[71] C. Gros, K. Hamacher, and W. Wenzel, Europhys. Lett. **69**, 616 (2005).
[72] J. B. Marston, J. O. Fjaerestad, and A. Sudbo, Phys. Rev. Lett. **89**, 056404 (2002).

[73] J. O. Fjærestad and J. B. Marston, Phys. Rev. B **65**, 125106 (2002).
[74] T. Vuletic, B. Korin-Hamzic, T. Ivek, S. Tomic, B. Gorshunov, M. Dressel, and J. Akimitsu, Phys. Rep. **428**, 169 (2006).
[75] A. Rusydi, P. Abbamonte, H. Eisaki, Y. Fujimaki, G. Blumberg, S. Uchida, and G. A. Sawatzky, Phys. Rev. Lett. **97**, 016403 (2006).
[76] B. Gorshunov, P. Haas, T. Rõõm, M. Dressel, T. Vuletić, B. Korin-Hamzić, S.Tomić, J. Akimitsu, and T. Nagata, Phys. Rev. B **66**, 060508(R) (2002).
[77] M. Tsuchiizu and Y. Suzumura, J. Phys. Soc. Jpn. **73**, 804 (2004).
[78] P. Abbamonte, G. Blumberg, A. Rusydi, A. Gozar, P. Evans, T. Siegrist, L. Venema, H. Eisaki, E. Isaacs, and G. Sawatzky, Nature (London) **431**, 1078 (2004).
[79] A. Rusydi, M. Berciu, P. Abbamonte, S. Smadici, H. Eisaki, Y. Fujimaki, S. Uchida, M. Rubhausen, and G. A. Sawatzky, Phys. Rev. B **75**, 104510 (2007).
[80] H. J. Schulz, Phys. Rev. B **34**, 6372 (1986).
[81] R. Konik and A. W. W. Ludwig, Phys. Rev. B **64**, 155112 (2001).
[82] F. H. L. Essler and R. M. Konik, Phys. Rev. B **75**, 144403 (2007).
[83] D. G. Shelton, A. A. Nersesyan, and A. M. Tsvelik, Phys. Rev. B **53**, 8521 (1996).
[84] B. Dumoulin, C. Bourbonnais, S. Ravy, J. P. Pouget, and C. Coulon, Phys. Rev. Lett. **76**, 1360 (1996).
[85] F. H. L. Essler and A. M. Tsvelik, Phys. Rev. B **65**, 115117 (2002).
[86] J. Voit, Eur. Phys. J. B **5**, 505 (1998).
[87] A. Iucci, G. A. Fiete, and T. Giamarchi, Phys. Rev. B **75**, 205116 (2007).
[88] V. Brunel, M. Bocquet, and T. Jolicoeur, Phys. Rev. Lett. **83**, 2821 (1999).
[89] T. Becker, M. Gabay, and T. Giamarchi, Phys. Rev. B **62**, 12489 (2000).
[90] D. A. Ivanov and P. A. Lee, Phys. Rev. B **59**, 4803 (1999).